FORMATION AND EVOLUTION OF BREATHERS IN A CHAIN OF NONLINEAR COUPLED OSCILLATORS

A THESIS SUBMITTED TO
THE GRADUATE SCHOOL OF NATURAL AND APPLIED SCIENCES
OF
THE MIDDLE EAST TECHNICAL UNIVERSITY

BY

HASAN GÜÇLÜ

IN PARTIAL FULFILLMENT OF THE REQUIREMENTS FOR THE

DEGREE OF

MASTER OF SCIENCE

IN

THE DEPARTMENT OF PHYSICS

JANUARY 2001

Approval of the Graduate School of Natural and Applied Sciences.

Prof. Dr. Tayfur Öztürk
Director

I certify that this thesis satisfies all the requirements as a thesis for the degree of Master of Science.

Prof. Dr. Sinan Bilikmen
Head of Department

This is to certify that we have read this thesis and that in our opinion it is fully adequate, in scope and quality, as a thesis for the degree of Master of Science.

Prof. Dr. Sinan Bilikmen
Supervisor

Examining Committee Members

Prof. Dr. Sinan Bilikmen _____

Prof. Dr. Ordal Demokan _____

Prof. Dr. Cevdet Tezcan _____

Assoc. Prof. Dr. Serhat Çakır _____

Assoc. Prof. Dr. Sibel Başkal _____

ABSTRACT

FORMATION AND EVOLUTION OF BREATHERS IN A CHAIN OF NONLINEAR COUPLED OSCILLATORS

Güçlü, Hasan

M.Sc., Department of Physics

Supervisor: Prof. Dr. Sinan Bilikmen

January 2001, 93 pages.

I study the formation and evolution of chaotic breathers (CB's) on the Fermi-Pasta-Ulam oscillator chain with quartic nonlinearity (FPU-β system). Starting with most of the energy in a single high frequency mode, the mode is found to break up on a fast time scale into a number of spatially localized structures which, on a slower time scale, coalesce into a single structure, a CB. On a usually longer time scale, depending strongly on the energy, the CB gives up its energy to lower frequency modes, approaching energy equipartition among modes. I analyze the behavior, theoretically, using an envelope approximation to the discrete chain of oscillators. For fixed boundaries, periodic nonlinear solutions are found, which are analyzed for linear stability. The stability analysis indicates that, for the usually narrow equilibrium structures, weakly unstable growth near peak amplitude would propagate into stable regions, thus not leading to large amplitude effects. However, broader mode initial conditions, which relax toward equilibria, may break up into symmetries other than that initially imposed. The

structures formed after the fast breakup are found to approximate the underlying equilibrium. The structures undergo slow translational motions, and an estimated time for them to coalesce into a single chaotic breather are found to agree with the numerically determined scaling $\tau_B \propto E^{-1}$. A previously developed theory of the decay of the CB amplitude to approach equipartition is modified to explicitly consider the interaction of the breather with background modes. The scaling to equipartition of $T_{eq} \propto E^{-2}$ agrees with the numerical scaling and gives the correct order of magnitude of T_{eq}.

Keywords: Nonlinear, Oscillator Chain, Breather, FPU, Fermi Pasta Ulam

ÖZ

LİNEER OLMAYAN OSİLATÖR DİZİSİNDE ESAS LOKALİZE MODLARIN OLUŞUM ve EVRİMİ

Güçlü, Hasan
Yüksek Lisans , Fizik Bölümü
Tez Yöneticisi: Prof. Dr. Sinan Bilikmen

Ocak 2001, 93 sayfa.

Bu tezde lineer olmayan dördüncü dereceden Fermi-Pasta-Ulam osilatör dizisinde (FPU-β sistemi) kaotik esas lokalize modların oluşum ve evrimi incelenmiştir. Yüksek frekanslı tek bir moda verilen enerjiyle başlatılan sistem kısa bir sürede çok sayıda lokalize yapıya ayrılmış, ilerleyen zamanla bu yapılar birleşerek tek bir yapıyı , kaotik esas modu oluşturmuştur. Kaotik esas mod ilk enerjiye bağlı olarak modlar arasında eşpaylaşıma giderek enerjisini daha düşük frekanslı modlara vermiştir. Bu davranış zarf fonksiyonu yaklaşımı kullanılarak teorik olarak incelenmiştir. Sabit sınırlar için lineer olmayan periyodik çözümler bulunmuş ve lineer kararlılık incelenmiştir. Kararlılık analizi genellikle dar denge yapıları için yüksek genlikli kararsız zayıf yapının kararlı bölgeye doğru ilerlediğini ve böylece yüksek genlik etkisine neden olmadığını göstermiştir. Bununla birlikte sistemi eşpaylaşıma götüren geniş ilk şartların daha önce öngörülmemiş simetrilere dönüşebileceği gözlemlenmiştir. Bu dönüşümden sonra oluşan yapıların sistemi eşpaylaşıma

yaklaştırdığı bulunmuştur. Tek bir esas lokalize mod oluşum süresinin sisteme ilk verilen enerjiyle ters orantılı olduğu ($\tau_M \propto E^{-1}$) nümerik olarak bulunmuş ve teoriyle uyumu tartışılmıştır. Esas lokalize modun eşpaylaşıma indirgenmesiyle ilgili daha önce geliştirilmiş bir teori, esas modun arkaplan modlarla etkileşimi gözönünde tutularak iyileştirilmiştir. Eşpaylaşıma gidiş süresinin ise ilk sistem enerjisinin karesiyle ters orantılı olduğu gözlenmiştir ($T_{ep} \propto E^{-2}$).

Anahtar Kelimeler: Osilatör Dizisi, Esas Lokalize Mod, FPU, Fermi Pasta Ulam

To the memories of former physicists.

ACKNOWLEDGMENTS

Any work of this sort necessarily represents the influence and help of many people. First of all I am indebted to my family for their love. I thank my Sinan Bilikmen for his continuing support throughout my physics education. I would like to thank Vladimir Mirnov who instilled in me a love of this discipline and helped writing this thesis. Special thanks to Tülün Ergin for her small but significant help in latex. I also thank Kai Ullman whose numerical code has been used in computational part of this work. I am also grateful to the founders of GNU for their great c++ compiler and to FreeBSD core team for their reliable operating system. Thanks also go to PB Sistem Limited for giving me some CPU time of their ultrafast machine, PBServer0. Finally I must give the biggest thanks to my mentor and friend, Osman Can, for his advices.

TABLE OF CONTENTS

LIST OF FIGURES

FIGURE

CHAPTER 1

INTRODUCTION

Coupled oscillator chains form good test systems for investigating energy exchange among degrees of freedoms [1]. In particular, the Fermi-Pasta-Ulam (FPU) system, consisting of a set of equal masses coupled to nearest neighbors by nonlinear springs, has been extensively studied [1, 2, 3, 4, 5, 6, 7, 8, 9, 10, 11, 14, 18, 19]. Starting with energy initially in a low frequency mode, Fermi, Pasta, Ulam [2] observed, for low energies, that the oscillators did not relax to the equipartition state, but displayed recurrences which were later explained in terms of beating among the system modes [1, 3]. A theoretical prediction of a threshold to fast equipartition by mode overlap [4] was subsequently qualitatively confirmed by studies of energy thresholds required to give approximate equipartition among modes [5, 6, 7]. A weaker mechanism that also led to equipartition on a slower timescale has also been studied [8, 9, 10]. With initial energy in a low-frequency mode, it was shown in [9] that the resonant interaction of a few low frequency modes can lead to local superperiod beat oscillation that is stochastic, transferring energy to

high frequency modes by diffusion. With increasing local energy, there is a transition from exponentially slow transfer to a time scale that is inversely proportional to a power of the energy density.

The FPU -β system with quartic nonlinearity can be approximated, for low-frequency mode initial conditions, by the mKDV equation, which admits a soliton solution, that can become unstable with increasing energy [11]. This instability roughly coincides with the creation of stochastic layers in the beat oscillations [9]. The close connection between the development of stochastic layers in beat oscillations and instabilities in nonlinear structures was also noted for the discretized sine-Gordon equation, consisting of pendula coupled by linear springs [12, 13]. In [12], it was numerically found that the breakup of a nonlinear structure, starting from a high-frequency mode initial condition, occurred at higher energy and on a slower time scale than from energy initially in a low-frequency mode.

A partial understanding of the increased stability came from a series of analyses of breather-like structures on discrete systems that admitted exact breather solutions [14, 15, 16, 17, 18, 19]. High frequency mode initial conditions have symmetry of neighboring oscillators close to that of localized exact breathers. The resulting dynamics consists of three stages. First there is an initial first stage in which the mode breaks up into a number of

breather-like structures. Second, on a slower time scale, these structures coalesce into one large unstable structure. These structures have been called chaotic breathers (CB) [18]. Since a single large CB closely approximates a stable breather, the final decay stage, toward equipartition, can be very slow. This behavior has been observed in oscillator chains approximating the Klein-Gordon equation with various force-laws [15, 16, 17] e.g. the discretized sine-Gordon equation [17], and, more relevantly for this thesis, the FPU-β model [14, 18, 19]. In [14] and [18], the energy was placed in the highest frequency mode with strict alternation of the amplitudes from one oscillator to the next. This configuration is stable up to a particular energy at which a parametric instability occurs, leading to the events described above [14, 18]. However, the nonlinear evolution does not depend on special initial conditions, but will generically evolve from any high-frequency mode initial condition that has predominantly the alternating amplitude symmetry [19]. One does not know, in this generic situation, whether there exists any true energy threshold to achieve equipartition, although there appears to be some numerical evidence for such a threshold in the discretized sine-Gordon system [12]. However, as discussed extensively with respect to low-frequency mode initial conditions, the practical thresholds refer to observable time scales [9, 10]. From a phase-space perspective it is intuitively reasonable that for a large number of oscillators and not too low an

initial energy the generic set of initial conditions will lie in a chaotic layer, but the chaotic motion can remain close to a regular orbit for very long times [1]. The scaling with energy density of the time to equipartition has been estimated for high frequency initial conditions, from the interaction of beat modes using a procedure developed to calculate the equipartition time from low frequency initial conditions [20]. The result gave the numerically observed scaling but strongly underestimated the time, which is at least partially related to the transient formation of the breather [19].

Considerable insight into the behavior of a nonlinear oscillator chain, starting from high frequency mode initial conditions, can be obtained by introducing an envelope function for the displacements of the oscillators. The initial conditions for the envelope only contain significant long wavelength perturbations. For the envelope function an expansion is then possible to obtain a nonlinear partial differential equation (PDE) which approximates the behavior of the discrete system [21, 22]. Low-order expansions of this type produce PDEs that have integrable solutions in the form of envelope solutions, analogous to the solutions produced from low-frequency initial conditions [21]. Higher order terms destroy the integrability, but the actual discretized oscillator chains can have localized breather solutions which are also integrable [16, 17]. Thus we might expect the results, obtained from

higher order expansions, to approximate breather solutions that may, however, be weakly unstable.

The envelope function expansion procedure has been applied to the FPU-β system to explore the nonlinear long-wavelength solution, its modulation instability, the localization into proto-breathers, and their coalescence into a single chaotic breather [22]. These results were mainly limited to the small-amplitude nonlinear solution, which therefore limited the range of applicability. The initial breakup of the high frequency mode was also calculated only for periodic boundary conditions, i.e. for the highest mode number for which the initial envelope function is uniform. These limitations led to results that, while qualitatively significant, do not agree quantitatively with numerical results in the usually explored energy density ranges or with oscillator chains with fixed ends [18, 19].

In the following chapters i first presented the basic equations of the chain in oscillator and normal mode forms. I then used expansions to obtain the envelope equation. Then, in Chaper III, i obtained solutions of the envelope equations valid for arbitrary amplitude. In Chapter IV i obtained the approximate local dispersion for the modulation instability and compare the results to numerical evolution of the discrete equations for a range of energies and initial periodicities of the envelope. Chapter V considers

coalescence of the protobreathers that are formed in the modulational instability process. In Chapter VI the mode picture of the energy transfer mechanism is modified to specifically take into account the beating between background low amplitude modes and the breather, to obtain an estimate of the breather decay time.

CHAPTER 2

BASIC EQUATION AND INITIAL CONDITIONS

The Hamiltonian function of the FPU-β model of N oscillators is

$$H = \sum_{i=0}^{N} \left[\frac{p_i^2}{2\ m} + \frac{K_h}{2}\ (q_{i+1} - q_i)^2 + \frac{K_{ah}}{4}\ (q_{i+1} - q_i)^4 \right] \tag{2.1}$$

where K_h and K_{ah} are, respectively, the harmonic and anharmonic force constants. This problem has fixed boundaries $p_0 = p_{N+1} = 0$, $q_0 = q_{N+1} = 0$. Using Hamilton's equations, the Hamiltonian yields the equations of motion of the individual oscillators

$$m\frac{d^2 q_i}{dt^2} = K_h(q_{i+1} + q_{i-1} - 2q_i) + K_{ah}[(q_{i+1} - q_i)^3 - (q_i - q_{i-1})^3] \quad i = 1,\ 2,\ ...N \tag{2.2}$$

Introducing dimensionless variables $t \rightarrow t\sqrt{K_h/m}$, $q \rightarrow q\sqrt{K_{ah}/(K_h\ \beta)}$ expressions (2.1) and (2.2) can be rewritten in the form that corresponds to $m = K_h = 1$.

$$H = \sum_{i=0}^{N} \left[\frac{1}{2}\ p_i^2 + \frac{1}{2}\ (q_{i+1} - q_i)^2 + \frac{\beta}{4}\ (q_{i+1} - q_i)^4 \right] \tag{2.3}$$

$$\frac{d^2 q_i}{dt^2} = q_{i+1} + q_{i-1} - 2q_i + \beta[(q_{i+1} - q_i)^3 - (q_i - q_{i-1})^3] \quad i = 1,\ 2,\ ...N \tag{2.4}$$

The dimensionless factor β is introduced to write (2.3) and (2.4) in a standard form which is traditionally used in publications for the FPU-β model. I choose $\beta = 0.1$ to correspond to previous papers and thus facilitate comparison with the results of other studies. The choice of β rescales the dimensionless variables such that the energy of the system and, correspondingly, the Hamiltonian are measured in the units of $\beta\ K_h^2/K_{ah}$

The Hamiltonian function (2.3) consists of quadratic part H_h which describes the harmonic oscillations and anharmonic quartic potential, H_{ah}, which is proportional to β. With the help of a canonical transformation H_h can be presented in the form of N independent normal modes P_j, Q_j

$$Q_j = \left(\frac{2\ \Omega_j}{N+1}\right)^{1/2} \sum_{i=1}^{N}\ \sin(k\ i\ j) q_i \tag{2.5}$$

$$P_j = \left(\frac{2}{\Omega_j (N+1)}\right)^{1/2} \sum_{i=1}^{N}\ \sin(k\ i\ j)\ \ p_i \tag{2.6}$$

such that the linear part of the Hamiltonian becomes

$$H_h = \sum_{j=1}^{N}\ \frac{\Omega_j}{2}\ (\ P_j\ ^2 + Q_j\ ^2) \tag{2.7}$$

where

$$\Omega_j = 2\ \sin\ \left(\frac{1}{2}\ k\ j\right),\quad k = \pi/(N+1), \qquad j = 1,\ 2, ...N \tag{2.8}$$

The reverse transformation is

$$q_i = \left(\frac{2}{N+1}\right)^{1/2} \sum_{j=1}^{N}\ \sin(k\ i\ j) \frac{Q_j}{\Omega_j\ ^{1/2}} \tag{2.9}$$

$$p_i = \left(\frac{2}{N+1}\right)^{1/2} \sum_{j=1}^{N} \sin(k\ i\ j)\ {\Omega_j}^{1/2}\ P_j \tag{2.10}$$

Index i is used for functions describing oscillators while j is used to label the variables related to the normal modes. Transformations (2.9),(2.10) automatically satisfy boundary conditions $p_0 = p_{N+1} = q_0 = q_{N+1} = 0$ which are kept fixed.

For numerical integration initial conditions are usually chosen such that at $t = 0$ only one normal mode is excited. If there were no nonlinear interaction between the normal modes the energy would be localized in this initially excited mode forever. However, due to anharmonic coupling the energy transfers throughout the spectrum. The purpose of this thesis is to examine the main physical mechanisms that partake in the processes of energy transfer.

In order to excite specifically one normal mode with the frequency Ω_γ the displacements of the oscillators and their momenta are chosen at $t = 0$ in accordance with (2.9), (2.10). The total energy E is shared between kinetic and potential parts of (2.7) such that a fraction f is delivered to the kinetic energy $P_\gamma^2(0) = 2\ f\ E/\ \Omega_\gamma$ while the rest of the energy is placed in the potential energy,

$$Q_\gamma^2(0) = \frac{1}{6\beta\Omega_\gamma}\left(\sqrt{24\beta E(1-f)(N+1) + (N+1)^2} - N - 1\right) \tag{2.11}$$

Expression (2.11) is calculated with the help of (2.3) and takes into

account the anharmonic term not included in (2.7). Correspondingly, the initial displacements and velocities of the oscillators are as follows:

$$q_i(0) = \left(\frac{2\ Q_\gamma^2(0)}{\Omega_\gamma(N+1)}\right)^{1/2} (-1)^{i+1}\ \sin\left(\frac{\pi\ i\ n}{N+1}\right) \tag{2.12}$$

$$\dot{q}(0)\ = p_i(0) = \left(\frac{2\ P_\gamma^2(0)\ \Omega_\gamma}{N+1}\right)^{1/2} (-1)^{i+1}\ \sin\left(\frac{\pi\ i\ n}{N+1}\right) \tag{2.13}$$

I will mostly treat the case $N = 128$ with initially excited mode $\gamma = 120$; however, other variants with different values of N, γ are also considered. I principally examine cases with γ in the upper part of the spectrum so that $n = N + 1 - \gamma << N + 1$. Note that for these cases the characteristic times of the initially excited modes correspond to a period $T \simeq \pi$, e.g. the frequency $\Omega_{120} \simeq 2$. In numerical calculations a small fraction of the total energy (10 percent) is usually placed into two satellites $\gamma - 1$ and $\gamma + 1$ to speed up the initial phase of the relaxation; however, this does not play an important role in long term behavior of the system.

The main parameter which defines the rates of the different stages of relaxation is the specific energy per oscillator E/N. For an intuitive understanding of this statement one can introduce new dimensionless functions $q_i \to q/\tilde{q}$ where $\tilde{q} = \sqrt{E/(N+1)}$. This leads to a slightly modified set of equations (2.4) with renormalized $\beta \to \beta\ [\ E/(N+1)\ ]$ which leaves the

R.H.S. of the new initial conditions for $q_i(0)$ and $dq_i/dt(0)$ independent of E/N and ranged between -1 and 1 for all possible values of N. Although a dependence on N still exists in the initial conditions it apparently becomes rather weak for large N such that the main parameter which defines the time scales of the relaxation explicitly depends on the specific initial energy per oscillator E/N. This general behavior was confirmed in the numerical calculations performed for different E/N and N [18, 19] . These calculations demonstrated that the long-term dynamics of relaxation was essentially independent of N for $N \gtrsim 100$.

A typical profile of initial displacements (2.12) is shown in Fig. 2.1 for the case $E = 50$, $f = 0$, $\gamma = 120$, exhibiting the fast variations of q_i from one oscillator to another characteristic of high γ modes. As in previous studies [21, 22], to remove this fast variations i introduce the envelope function $\psi_i(t) = (-1)^i \; q_i(t)$ which is a slowly varying function of the number i. The profile of the complete envelope function corresponding to Fig. 2.1 is illustrated in Fig. 2.2. The smooth spatial profile of ψ makes possible the use of a continuous approximation where the oscillators are described by the continuous variable $x = ai$, where a is the lattice period. Taylor's expansion then gives

$$\psi(x \pm a) = \psi(x) + \psi_x(x)(\pm a) \; + (1/2)\psi_{xx}(x) \; a^2 \; + \\ (1/6)\psi_{xxx}(x)(\pm a)^3 \; + (1/24)\psi_{xxxx}(x) \; a^4 \; + ... \qquad (2.14)$$

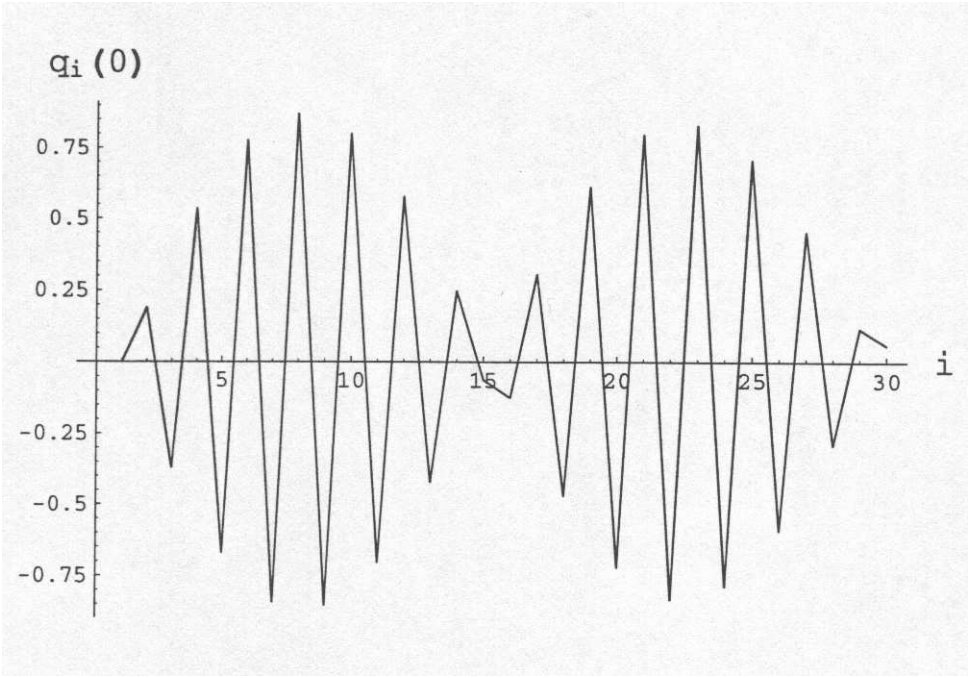

Figure 2.1: Initial displacements q_i for the first 30 oscillators ($i = 1,\ 2\ ...30$) out of $N = 128$ in the case $E = 50$, $\gamma = 120,\ \ n = N + 1 - \gamma = 9$. The mode has the symmetry that left and right oscillators (with respect to the central one) have displacements of almost equal amplitude but opposite sign.

Substituting (2.14) in (2.4) and collecting terms proportional to the different powers of a yields

$$\psi_{tt} + 4\ \psi\ +\ 16\ \beta\ \psi^3 + a^2\ \{\ \psi_{xx} + \beta\ (12\ \psi\ \psi_x^2\ +\ 12\ \psi^2 \psi_{xx})\}\ +$$

$$a^4\ \{\ (1/12)\ \psi_{xxxx} + \beta\ (3\ \psi_x^2\ \psi_{xx} + 3\psi\psi_{xx}^2\ +\ 4\psi\psi_x\psi_{xxx}\ +\ \psi^2\ \psi_{xxxx})\} + ... = 0 \tag{2.15}$$

where subscripts t and x stand for temporal and spatial derivatives of $\psi(x,t)$. Linear terms with spatial derivatives describe the dispersion (dependence of Ω on effective wave number $\pi j/(N+1)$ in (2.8)). Nonlinear

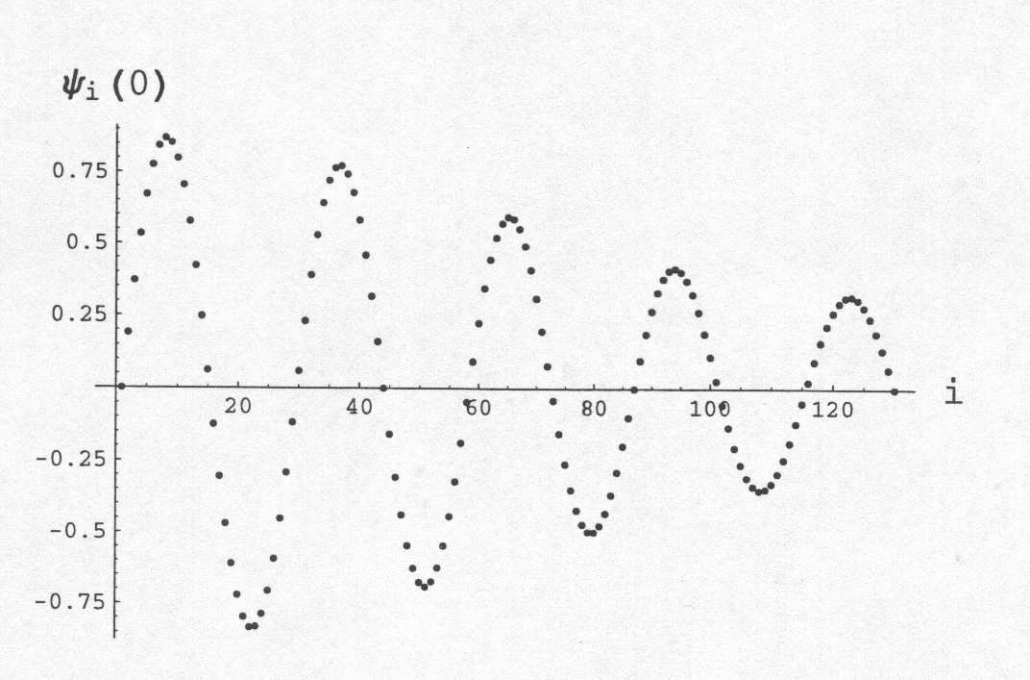

Figure 2.2: The plot of the envelope function $\psi_i = (-1)^i q_i(0)$ at initial time $t = 0$, $N = 128$, $\gamma = 120$. Nine extrema correspond to $n = N + 1 - \gamma = 9$. The smooth decrease of ψ_i from left to right results from the fact that in numerical simulations a small amount of energy ($\sim 10\%$) was placed in two nearest neighbor modes $\gamma = 119$ and $\gamma = 121$.

terms produce a frequency shift, which drives a process of steepening of the envelope function and formation of localized states (CB's), while the effect of dispersion leads to the opposite process of flattening of the envelope function. This qualitatively explains why relaxation is accompanied by the formation of sharply localized states if energy is initially deposited in the high frequency part of the spectrum where the effect of dispersion is small, while only broad nonlinear structures are formed if the energy is initially in the low frequency modes where the dispersion is large.

CHAPTER 3

SOLUTIONS FOR THE ENVELOPE FUNCTION

In (2.15), neglecting the terms with a^6 or higher , introducing the dimensionless variable $x \to x/a$ $(0 \leq x \leq N+1)$ and assuming a monochromatic dependence $\psi(x,t) = \psi(x)\cos\omega\ t$ leads to an equation for $\psi(x)$ (where ω plays role of the eigenvalue)

$$(-\omega^2+4)\ \psi\ +\ \psi_{xx}\ +\ \beta\ (\ 12\ \psi^3\ +\ 9\ \psi\ \psi_x^2\ +\ 9\ \psi^2\psi_{xx})\ +$$

$$(1/12)(\ \psi_{xxxx} + \beta\ (27\ \psi_x^2\ \psi_{xx} + 27\psi\psi_{xx}^2\ +\ 36\psi\psi_x\psi_{xxx}\ +\ 9\psi^2\ \psi_{xxxx}))\ =\ 0 \tag{3.1}$$

where i have used $\cos^3\ \omega\ t = (3/4)\ \cos\omega\ t\ + (1/4)\ \cos 3\ \omega\ t$ with terms proportional to $\cos 3\ \omega\ t$ ignored [21, 22]. This is also known as rotating wave approximation (RWA). Neglecting terms proportional to β yields a linear equation for the eigenmodes:

$$(-\omega^2+4)\ \psi\ +\ \psi_{xx} = 0 \tag{3.2}$$

Solving this equation for $\psi(x)$ with zero boundary conditions at $x = 0$ and $x = N+1$ gives N eigenmodes which correspond to the high frequency linear

normal modes of the discrete FPU chain

$$\psi_n{}^{(0)}(x) = \psi_{mn} \ \sin q_n \ x \tag{3.3}$$

$$\omega^2 \ = \ 4 - q_n^2, \qquad q_n = \frac{\pi(N+1-\gamma)}{N+1} = \frac{\pi \ n}{N+1} \tag{3.4}$$

where $n = N + 1 - \gamma \ll N + 1$ and $\psi_{mn} \equiv \psi_{max,\ n}$. Superscript (0) is introduced to indicate that (3.3) is a solution to the linearized equation (3.2).

The reduced (with all terms of order a^4 dropped) nonlinear equation (3.1) has exact analytical solutions, $\psi(x)$, which are periodic functions of x. A subset of these solutions have $q = 0$ at $x = 0, N + 1$. These solutions are a natural generalization of the linear solutions, for the case when nonlinear effects are important. These envelope functions have the same spatial periodicity as the corresponding linear modes (3.3). However, their profiles are not harmonic functions of x and the frequency of oscillations has a nonlinear shift. Note that the third (and higher) harmonics of ω, which are excluded from consideration due to the RWA, leads to nonharmonic time dependence of $\psi(x,t)$. Multiplying (3.1) by ψ_x, and integrating over x yields a first integral

$$(-\omega^2 + 4) \ \psi^2 \ + \ {\psi_x}^2 \ + \ \beta \ (\ 6 \ \psi^4 \ + \ 9 \ \psi^2 \ \psi_x^2) \ = C_1 \tag{3.5}$$

where all terms of order a^4 have been dropped.

This function describes a family of solutions which depends on two parameters, C_1 and ω. Equation (3.5) has been examined in the special case where C_1 is chosen such that $\psi_x = 0$ at $\psi = \psi_{max}$ and $\psi = \psi_{min}$ [22]. I consider more general cases assuming that $\psi_x = 0$ at $\psi = \psi_{max}$ but not using the second condition that $\psi_x = 0$ at $\psi = \psi_{min}$ (see, for example solution (3.3) for $n = 1$). Assuming that $\psi(x)$ is normalized to the maximum value $\psi_m \equiv \psi_{max}$, and introducing, correspondingly, a new function $f(x) \equiv \psi(x)/\psi_m$ one can rewrite 3.5 in a form which is similar to the energy conservation law for a unit mass particle in an external potential $U(f)$

$$\frac{{f_x}^2}{2} \; + \; U(f) = 0 \tag{3.6}$$

where ${f_x}^2$ plays role of kinetic energy while the potential energy is

$$U(f) \; = - \; \frac{3 \; \beta \psi_m^2 (1 - f^2)(\; f^2 \; + \; C_2)}{(1 \; + \; 9 \; \beta \; \psi_m^2 f^2)} \tag{3.7}$$

and the total energy is zero. In transforming from (3.5),(3.6) to (3.7) the relation $f_x = 0$ at $f = 1$ was used and a new constant $C_2 = (\; 4 - \omega^2 + 6 \; \beta \; \psi_m^2 \;) \; / \; 6 \beta \; \psi_m^2$ was introduced, replacing $C_1 = 6 \; \beta \psi_m^4 \; C_2$. The graphs of $U(f)$ are illustrated in Fig. 3.1. for three different values of the constant C_2 ($C_2 = -0.9, \;\; 0, \; 0.9$). Intersections of these graphs with the horizontal line $E = 0$ show that in the case of positive C_2 (for example, $C_2 = 0.9$) solutions $\psi(x)$ are oscillating functions of x which vary between minimum $-\psi_m$ and maximum ψ_m values. $C_2 = 0$ corresponds to the special separatrix solution

which is represented by the single localized wave (soliton, breather) with $\psi(x) \to 0$ at $x \to \pm\infty$ and frequency

$$\omega_B^2 = 4 + 6\ \beta\ \psi_m^2 \tag{3.8}$$

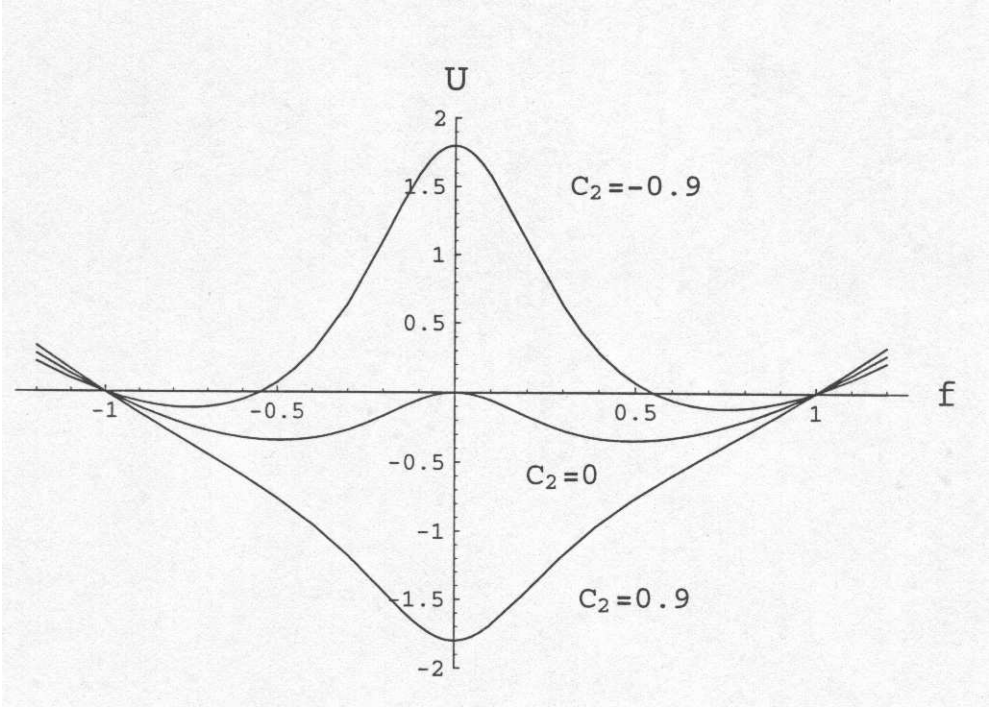

Figure 3.1: Graphs of the effective potential energy $U(f)$ as a function of f, $0 \leq f \leq 1$, for three values of the constant of integration C_2.

In the third case of negative C_2 solutions $\psi(x)$ are varying between two nonzero positive/negative boundaries ψ_{max} and ψ_{min} with frequency $\omega^2 = 4 + 6\ \beta\ (\psi_{min}^2 + \psi_{max}^2)$. This third family of solutions is related to the case of periodic nonzero boundary conditions, $q_1 = q_{N+1}$, mentioned above. In particular, when $C_2 \to\ -1$, it represents so called π - mode when each single oscillator is involved in coherent motion where its two neighbors have

opposite phases and equal amplitudes and, correspondingly, the envelope function $\psi = \psi_{max} = \psi_{min} = \psi_m$. In this case the nonlinear frequency shift reaches a maximum value

$$\omega^2 = 4 + 12\ \beta\psi_m^2 \tag{3.9}$$

which can be easily obtained from (2.4) by keeping $q_{i+1} = q_{i-1} = -q_i$.

In order to satisfy boundary conditions of fixed zero displacements at $x = 0$ and $x = N + 1$ the first case (positive C_2) is required since it is the only one which periodically passes though the point where $\psi = 0$. The spatial period of these oscillations is given by

$$\int_0^1\ df\ \left(\frac{df}{dx}\right)^{-1}\ =\ \Lambda/4 \tag{3.10}$$

Zero boundary condition at $x = N + 1$ is automatically satisfied if the half wave length $\Lambda/2$ is a solution to the equation $(\Lambda/2)\ n = N + 1$, where n is integer ($n\ =\ 1,\ 2...N$) and related to γ, as $n = N + 1 - \gamma$. The dispersion relation (3.10) determines the spectrum of the frequencies ω as a function of n and ψ_m. Substituting f_x from (3.6) in (3.10) and using a new variable $\sin\alpha = f$, (3.10) can be written in the form

$$I(r, \psi_m) = \frac{2}{\pi}\int_0^{\pi/2} d\alpha\ \left(\frac{1\ +\ 9\ \beta\ \psi_m^2\ \sin^2\alpha}{\sin^2\alpha\ +\ r^2}\right)^{1/2}\ =\ \sqrt{6\ \beta\ \psi_m^2\ \left(\frac{N+1}{\pi n}\right)^2} \tag{3.11}$$

where i have substituted $\lambda/4\ =\ (N\ +\ 1)/(2n)$ on the R.H.S. The factor $r^2 \equiv C_2 = (\ 4 - \omega^2 + 6\ \beta\ \psi_m^2\ )\ /\ 6\beta\ \psi_m^2$ has been introduced as a positive

quantity to provide convergence of the integral and, thus, to satisfy the boundary conditions. The parameter $w(n, \psi_m)$ on the R.H.S. of (3.11)

$$w(n, \psi_m) = 6\ \beta\ \psi_m^2\ \left(\frac{N+1}{\pi n}\right)^2 \tag{3.12}$$

gives the relative effect of the nonlinear frequency shift of a given normal mode of integer n, with respect to the linear frequency shift of that mode from the upper frequency bound. This factor plays an important role in nonlinear wave dynamics, describing the relationship between linear dispersion and nonlinear effects. The balance of these mechanisms leads to the spontaneous formation of transient self-consistent localized structures with $w \simeq 1$, which are observed in almost all numerical simulations.

The limiting case of weak nonlinearity corresponds to values of $w \ll 1$. This smallness can be balanced by the integral in the L.H.S. if $r \to \infty$. Simplifying the integrand in this limit, $I(r, \psi_m) \to 1/r$, yields a discrete spectrum of eigenfrequencies of the linear problem

$$\omega_n^2\ =\ 4\ +\ 6\ \beta\ \psi_m^2\ -\frac{\pi^2\ n^2}{(N+1)^2} \tag{3.13}$$

where the small nonlinear correction $6\ \beta\ \psi_m^2$ is added to the linear case (3.4).

In the opposite limiting case, $w(n, \psi_m) \gg 1$, one should solve the dispersion relation for the R.H.S. of (3.11) much greater than one. This can be balanced by the L.H.S. if $r \ll 1$. Asymptoticly expanding the L.H.S. for

$r \to 0$ yields a logarithmic dependence on r in the leading approximation which describes the dependence on ψ_m (see, Appendix A)

$$I(r, \psi_{max}) \to \frac{1}{\pi} \ln \left(\frac{16}{r^2 \ (1 + 9\beta\psi_m^2)} \right) + \frac{6 \ \sqrt{\beta\psi_m^2}}{\pi} \arcsin \sqrt{\frac{9\beta\psi_m^2}{1 + 9\beta\psi_m^2}} \quad (3.14)$$

Solving (3.11) for ω yields the spectrum of the eigenfrequencies valid in the case of strong nonlinearity

$$\omega_n^2 \ = \ 4 + 6\beta\psi_m^2 \left\{ 1 - \frac{16}{1 + 9\beta\psi_m^2} \exp \left[-\sqrt{6\beta\psi_m^2} \left(\frac{N+1}{n} - \sqrt{6} \arcsin \sqrt{\frac{9\beta\psi_m^2}{1 + 9 \ \beta\psi_m^2}} \right) \right] \right\} \quad (3.15)$$

The factor r^2 is given by the second term in curly brackets. It is exponentially small, $r^2 \propto \exp(-w/\pi)$, in the strongly nonlinear case, $w \gg 1$. The spatial profiles of the nonlinear eigenfunctions $\psi(x)$ are determined by the integral of (3.6), (3.7), having an upper limit given by $\arcsin(\psi/\psi_m)$ and zero boundary condition at $x = 0$ while the second zero boundary condition at $x = N + 1$ is satisfied automatically since ω_n is the eigenvalue given by the relation (3.11).

$$x(\psi) = \frac{1}{\sqrt{6 \ \beta \ \psi_m^2}} \int_0^{\arcsin(\psi/\psi_m)} d\alpha \ \left(\frac{1 \ + \ 9 \ \beta \ \psi_m^2 \ \sin^2 \alpha}{\sin^2 \alpha \ + \ r^2} \right)^{1/2} \qquad 0 \le x \le \Lambda/4 \quad (3.16)$$

Equation (3.16) defines $\psi(x)$ in $0 \le x \le \Lambda/4$. It is symmetrically continued from $\Lambda/4$ to $\Lambda/2$, then antisymmetrically reflected from $\Lambda/2$ to Λ, and then periodically continued over the entire chain. The resulting graphs of $\psi_n(x)$ are plotted in Figs. 3.2 and 3.3 together with the profiles of equivalent linear

modes (3.3) for typical values $N = 128, n = 9, \beta = 0.1$ and two amplitudes $\psi_m = 0.45$ and $\psi_m = 1.85$, respectively. These values correspond to weak and strong nonlinearity, $w(9, \psi_m) \simeq 3$ and $w(9, \psi_m) \simeq 50$, respectively. The linear profiles (3.3) are used for initial conditions. In the process of relaxation these initial profiles might be expected to approach the equivalent envelope solutions (3.16) of the same periodicity and total energy. Due to conservation of energy the amplitudes of the envelope solutions (3.16) are higher than the initial values. In the weakly nonlinear case 3.2 the difference is small, while in the strongly nonlinear case 3.3 the difference is large because the nonlinear peaks are much narrower than the initial sinusoidal profiles. Numerical calculations presented in the next chapter show that due to a modulation instability the periodicity is broken in the process of relaxation such that the only link between initial and final states is the conservation of energy.

The periodic envelope solution (3.16) with $n = 1$ looks similar to the single breather in an infinitively long chain, which is obtained from (3.16) in the limit $N \to \infty$. Putting $r = 0$ and rearranging the limits of integration in accordance with zero boundary conditions at infinity, yields

$$x(f) = \frac{1}{\sqrt{6\ \beta\ \psi_m^2}} \int_{\arcsin f}^{\pi/2} \frac{d\alpha}{\sin\alpha} (1\ +\ 9\ \beta\ \psi_m^2\ \sin^2\alpha)^{1/2} \qquad 0 \leq x < +\infty \tag{3.17}$$

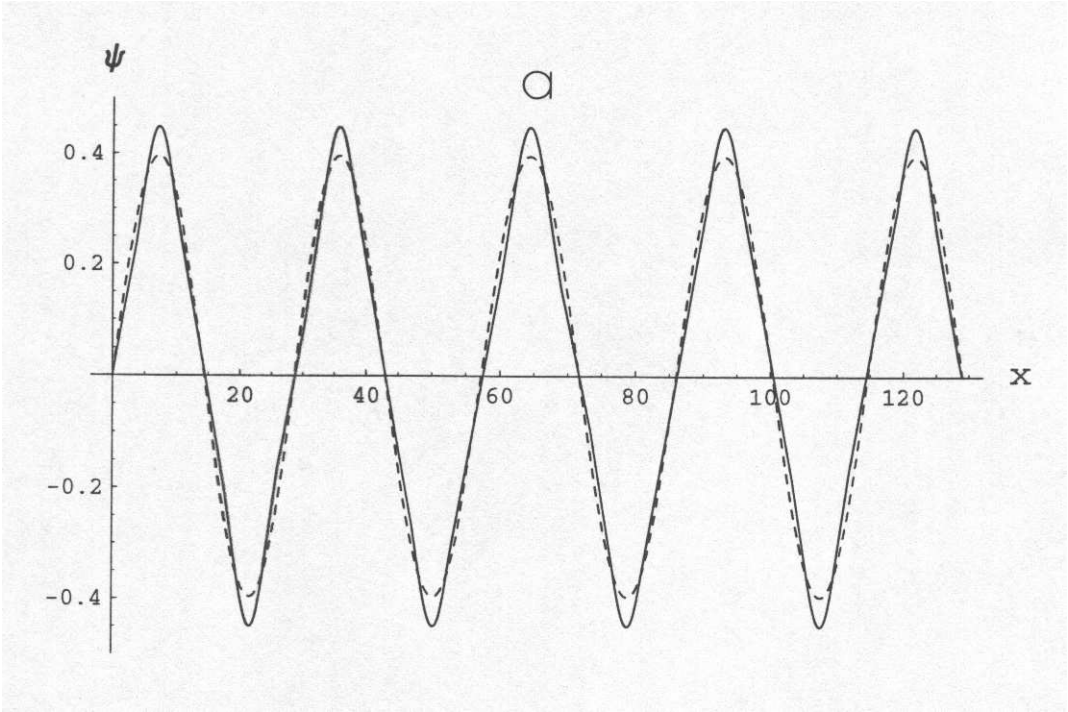

Figure 3.2: Comparison of the weakly nonlinear envelope solution (3.16) (solid line) with the equivalent profile of the normal mode (3.3) (dashed line) with energy $E = 20$ and symmetry $n = 9$. Since the factor $w \simeq 3$ is not too large , the curves are close to each other.

For the low amplitude case, $9\beta\psi_m^2 \ll 1$, integral (3.17) is simplified giving

$$\psi_B(x) \;=\; \psi_m \cosh^{-1}(\sqrt{6\ \beta}\ \psi_m\ x) \tag{3.18}$$

while in the large amplitude case, $9\beta\psi_m^2 \gg 1$, (3.17) describes, asymptotically, the breather of finite width $d \simeq 5$ (five oscillators)

$$\psi_B(x) \;=\; \psi_m \cos\sqrt{\frac{2}{3}}\ x \qquad\qquad -\pi\sqrt{\frac{3}{8}} < x < \pi\sqrt{\frac{3}{8}} \tag{3.19}$$

The energy of the envelope solutions is given by equation (B.4). The first two terms are calculated at the boundaries and cancel each other because of

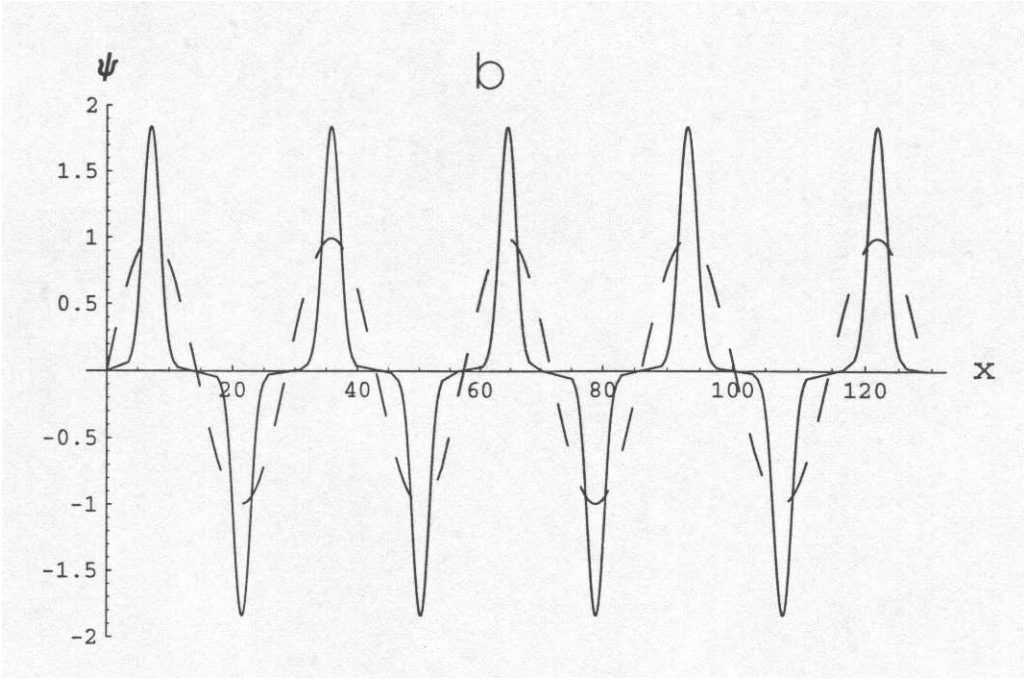

Figure 3.3: Comparison of the strongly nonlinear envelope solution (3.16) (solid line) with the equivalent profile of the normal mode (3.3) (dashed line) at energy $E = 200$ and symmetry $n = 9$. The large value of $w \simeq 50$ makes the curves significantly different.

the spatial periodicity of the modes. The last three terms in the integrand are ignored because they originate from terms of a^4 order in equation 2.15 which are not considered. Substituting (3.5), (3.6) into (B.4), expressing ω^2 in terms of r^2 and transforming the variable of integration as in (3.11) yields an expression for the energy

$$E = \frac{2\ n\ \psi_m}{\sqrt{6\beta}} \int_0^{\pi/2} d\alpha\ \left(\frac{1\ +\ 9\ \beta\ \psi_m^2\ \sin^2\alpha}{\sin^2\alpha\ +\ r^2} \right)^{1/2}\ \times$$

$$\times \left((3\ \beta\ \psi_m^2 \sin^4\alpha\ +\ 2\ \sin^2\alpha\ -\ \frac{3}{2}\ \beta\ \psi_m^2\ r^2 \right) \qquad (3.20)$$

The integral in (3.20) is simplified and calculated analytically in two limiting cases. If ψ_m is sufficiently high that, $w(n, \psi_m) \gg 1$, nonlinear effects are dominant in comparison with the effect of dispersion and according to (3.11), $r \to 0$. Substituting $r = 0$ in (3.20) the integral is calculated exactly and defines a function $Z(y)$ with $y = \beta\ \psi_m^2$. The explicit expression for $Z(y)$ is given by (B.5),(B.6). This function can be further simplified in the limits of $y >> 1$ and $y << 1$ which we call, respectively, large and small amplitude nonlinear envelopes. In the first subcase the asymptotic expansion of $Z(y)$ yields

$$E = \frac{9\ \pi\ \sqrt{6}\ n\ \beta}{16} \left(\psi_m^4 - \frac{2}{3\pi\sqrt{\beta}}\ \psi_m^3 \right), \qquad 1 \ll \sqrt{6\ \beta\ \psi_m^2} \tag{3.21}$$

where the ψ_m^3 term is the next order correction to the leading ψ_m^4 term. In this large amplitude regime energy is mostly due to the quartic β term in the potential energy (2.3). The envelope function and energy are concentrated in n narrow periodically distributed peaks each consisting of 4-5 oscillators while in wide areas between the peaks oscillations are exponentially small.

In the second subcase of small amplitude, the leading terms in the expansion of $Z(y)$ yield

$$E = \frac{4\ n}{\sqrt{6\ \beta}} \left(\psi_m + 4\ \beta\ \psi_m^3 \right) \qquad \pi\ n/(N+1) \ll \sqrt{6\ \beta\ \psi_m^2} \ll 1 \tag{3.22}$$

where the ψ_m^3 term is a correction to the leading, ψ_m term. The energy is mostly due to the quadratic term in the potential energy (2.3). It is

also localized in n periodically distributed peaks but the width of the peaks and, correspondingly, the number of oscillators in each of them are inversely proportional to ψ_m. This results in the linear dependence on ψ_m in (3.22).

If the amplitude ψ_m is sufficiently low that $\sqrt{6\ \beta\ \psi_m^2} \ll \pi n/(N+1)$ the oscillations become nearly linear. As in obtaining (3.13) the factor r is now much greater than one and integral (3.20) can be calculated in the limit $r \to \infty$ by ignoring the term $\sin\alpha$ in comparison with r in the denominator. Expression (3.20) yields

$$\frac{E}{N+1} = \psi_m^2 \left(1 - \frac{\pi^2 n^2}{4(N+1)^2}\right) \qquad \sqrt{6\ \beta\ \psi_m^2} \ll \pi\ n/(N+1) \ll 1 \quad (3.23)$$

The quadratic energy dependence on ψ_m again results from the quadratic term in the potential energy (2.3) with a maximum value of $2\ \psi_m^2$ in a single oscillator, and a factor of $1/2$ is introduced from the nonuniform profile of the envelope function. This regime is equivalent to the discreet normal mode solution, which represents initial conditions used in numerical calculations in the case when all energy is placed at $t = 0$ in the potential energy.

CHAPTER 4

FAST EVOLUTION FROM INITIAL STATES

For most numerical studies of oscillator chains the initial state imposed on the system is that of a single linear mode. This state is generally not close to an equilibrium. The initial state rapidly relaxes, governed by the nonlinear equations. The evolution may be influenced by the underlying stability of nearby equilibria, but cannot be analyzed directly as perturbations around those equilibria. It is also possible to prepare the initial conditions to be close to an equilibrium and consequently to directly analyze linear stability. I therefore study both the linear stability of the envelope solutions with respect to small perturbations, $\delta\psi_i(x) << \psi_i(x)$, and the relaxation from a remote initial state (2.12), (2.13) to nonlinear envelope solutions (3.16).

For analysis of non-stationary envelopes, which describe relaxation, instability, or breather translational motion, it is convenient to rewrite the basic equation (2.15) in the form of two coupled equations for amplitude $q(x,t)$ and phase $\phi(x,t)$ which are related to $\psi(x,t)$ as

$$\psi(x,t) = q(x,\ t)\ \cos(\omega\ t\ +\ \phi(x,t)) \tag{4.1}$$

Substituting (4.1) in (2.15) and collecting terms proportional to $\sin(\omega t + \phi(x,t))$ and $\cos(\omega t + \phi(x,t))$ leads to coupled equations for the phase $\phi(x,t)$ and amplidute $q(x,t)$

$$q\phi_{tt} + 2\ q_t(\omega + \phi_t) + 2\ q_x\phi_x + q\phi_{xx} + 12\ \beta q^2 q_x\phi_x + 3\ \beta q^3\phi_{xx} = 0 \quad (4.2)$$

$$q_{tt} - (\omega + \phi_t)^2 q + 4\ q + q_{xx} - q\phi_x^2 + 12\ \beta q^3 + 9\ \beta q(qq_x)_x - 6\ \beta q^3\phi_x^2 = 0 \quad (4.3)$$

4.1 Linear Analysis Of Stability

Envelope solutions are fast oscillating functions of time which are subject to parametric (modulation) instability. The instability is driven by the periodic variation of the frequency, which appears in the linear equation for a perturbation, due to the nonlinear frequency shift caused by the unperturbed envelope solution. For the usually applied modal initial conditions unstable breakup of modes are observed [18, 19]. However, numerical calculations show that the nonlinear stage of this instability leads to the formation of long living self-organized localized structures, chaotic breathers, which appear to be marginally stable with respect to a fast modulation instability. By investigating the stability of nonlinear equilibria i will improve our understanding of the mechanism by which they are stabilized. Although i am examining periodic equilibria (3.16), i will put significant attention to the limiting case, $w = \infty\ , r = 0$ that corresponds to a single breather in an infinitivly long chain of oscillators ($N \to \infty$).

A second problem is concerned with the question how many breathers appear after the relatively short time of nonlinear relaxation from the initial state. In this context my problem with fixed zero boundary conditions is significantly different from the usually applied π-mode initial values for periodic boundary conditions. In the periodic case the π-mode is simultaneously a normal mode of the linear problem and an exact solution to the nonlinear envelope equation (3.16). Relaxation from this equilibrium state is initiated by a modulation instability, and the wavelength of the fastest growing mode is used to estimate the number of breathers generated during the nonlinear phase of instability.

In the case of zero boundary conditions, high frequency normal modes (2.12), (2.13) do not satisfy the nonlinear envelope equation (3.5). When used as initial conditions they relax toward or around a few nearest stable equilibrium solutions (3.16) at $t > 0$. I expect that the linear analysis could, at best, only qualitatively describe the evolution of the system. Nevertheless, as we shall see, the linear analysis, in combination with numerical results, is quite useful for understanding evolution and quasistability of strongly nonlinear structures.

Comparing (4.1) to the unperturbed envelope solution $\psi(x,t) = \psi(x)\cos\omega t$, we see that the unperturbed phase is equal to zero, $\phi_0 = 0$, while the unperturbed amplitude is $q_0(x) = \psi(x)$. The frequency ω is a constant given by

(3.8) and determined by the amplitude of the unperturbed solution. When the amplitude is slightly varied, $q(x,t) = \psi(x) + \delta q(x,t)$, the frequency of the fast nonlinear oscillation is also varied. As ω is taken to be constant this effect is represented by the time-varying phase, $\phi(x,t) = \delta\phi(x,t)$. This phase difference can accumulate leading to large values of $\delta\phi(x,t)$. However, since equation (4.2) depends on derivatives of $\delta\phi(x,t)$ but not the phase by itself, it can be linearized by considering the derivatives of $\delta\phi(x,t)$ as first order corrections. This yields a system of two coupled linear equations

$$2\omega\delta q_t + \psi\ \delta\phi_{tt} + 2\ \psi_x\ (1 + 6\beta\psi^2)\ \delta\phi_x + \psi\ (1 + 3\ \beta\psi^2)\ \delta\phi_{xx} = 0 \qquad (4.4)$$

$$\delta q_{tt} + ((1+9\beta\psi^2)\ \delta q_x)_x + (4 - \omega^2 + 36\beta\psi^2 + 18\beta\psi\psi_{xx} + 9\beta\psi_x^2)\ \delta q - 2\omega\psi\delta\phi_t = 0 \qquad (4.5)$$

I first consider the simplest case of constant spatial profile of the envelope $\psi(x,t) = \psi_m\ cos\ \omega t$, which corresponds to π-mode with periodic boundary conditions, which has the highest nonlinear frequency shift (3.9) [22, 23]. This mode is a solution to (3.5) but does not belong to our envelope solutions because zero boundary conditons are not satisfied in this case. Setting the spatial derivatives of $\psi(x)$ equal to zero, (4.4) and (4.5) reduce to a system of coupled equations for $\delta\phi(x,t)$ and $\delta q(x,t)$ with constant coefficients. They can be solved by letting $\delta q(x,t) \propto \delta\phi(x,t) \propto \exp(st + i\ k\ x)$ which gives a

biqudratic equation for s:

$$s^4 + 2\,[\,36\,y+8-k^2(1+6\,y)\,]\,s^2 = k^2\,(1+3\,y)\,[\,24\,y-k^2\,(1+9\,y)]\quad (4.6)$$

where $y = \beta\psi_m^2$ as defined in Chapter III.

Among the four roots of (4.6) there is an unstable solution for which Re s is positive in two intervals of k. These intervals are; for small k, $k < \sqrt{24\,y\,/\,(1+9\,y)}$, $\lambda > 2\pi\sqrt{(1+9\,y)/24\,y}$, and for large k, $k > 2$, $\lambda < \pi$. The second interval, is beyond the validity of the continuous approximation so i will not consider it. At long wavelength, λ must be *apriori* less than $N+1$ in order to satisfy periodic boundary conditions. Using these inequalities, $2\pi\sqrt{(1+9\,y)/24y} < \lambda < N+1$, one can conclude that there is a threshold for the modulation instability of the π-mode

$$6\,\beta\,\psi_m^2\frac{(N+1)^2}{\pi^2} > 1 \qquad (4.7)$$

Near this threshold the factor $9\,y \ll 1$ and has therefore been dropped. Expression (4.7) shows that the π-mode is parametrically unstable if the nonlinear parameter (3.12), for $n = 1$, is greater than one. If (4.7) is satisfied, there is a most unstable wavenumber k_m which corresponds to the maximum of the growth rate, s_m. In the limit of small f_m, $y \ll 1$, the values of k_m and s_m were found in [22]

$$k_m = \sqrt{12\beta}\;\psi_m, \qquad s_m = 3\beta\psi_m^2 \qquad (4.8)$$

However, i am mainly interested in the cases of intermediate and large amplitude envelopes. In order to analyze these regimes all terms following from (3.11) are included in (4.6). In the limit of large amplitudes, $y \gg 1$, the fastest growing mode has wavenumber and maximum growth rate

$$k_m = 1.23, \qquad s_m = 0.93\ \sqrt{\beta}\ \psi_m \tag{4.9}$$

In contrast to the case of the low amplitude results in (4.8), k_m is independent of the amplitude and s_m is a linear function of ψ_m. Note that the transition from small to large amplitude takes place at $\beta\ \psi_m^2 \simeq 1/9$ that corresponds, for $\beta = 0.1$, to $\psi_m \simeq 1$.

The modulation instability of the envelope solutions obtained in Chapter III requires a more complicated analysis because the unperturbed functions $\psi(x)$ lead to x-dependent terms in (4.4) and (4.5). Full analysis of the problem can be done on the basis of eigenfunctions satisfying zero boundary conditions. I limit my study to instability of nonuniform envelope solutions with respect to short wavelength perturbations which most generally have the form

$$\delta\phi(x,t),\ \delta q(x,t) \propto \exp(s\ t + i \int_0^x k(x')\ dx') \tag{4.10}$$

with $k \gg \psi_x/\psi, \quad k^2 \gg \psi_{xx}/\psi$, which gives a qualitative understanding of the effect of spatial variations. I examine the local stability of the envelope solutions assuming that the perturbations 4.9 are localized in some area

of width D, $k^{-1} \ll D \ll d$, where $d^{-1} \simeq \psi_x/\psi$ is a typical scale of the unperturbed solution, and form a wave packet with central wave number k. The growth rate s is then calculated as a function of x and k. The result indicates what parts of the envelope profile $\psi(x)$ are locally stable or unstable and therefore where the instability can occur dependending on the local position of the wave packet in x and the local values of k. This approach does not take into account the boundary conditions and it is valid if the wave packet group velocity v_{gr} is small enough, so that $v_{gr}/s \ll d$. Following this program i analyze the stability of a single breather in the limit of small, amplitude, 9 $y << 1$, and large amplitude, $9y >> 1$, using, respectively, approximations (3.18) or (3.19).

For low amplitude from (4.8) for the π-mode i have only values of ψ_m such that s is small compared to the frequency $\omega \geq 2$ of the breather. These slowly varying perturbations can be treated on the basis of a reduced form of equations (4.4) and (4.5) with the terms $\delta\phi_{tt}$ and δq_{tt} ignored. Moreover, as can be shown from (3.6),(3.7) the terms proportional to ψ_x^2 and $\psi\psi_{xx}$ are proportional to $6\beta\psi_m^4$ and therefore small in comparison with $\psi^2(x)$ and can be neglected. Among the small perturbation terms i will keep the two terms proportional to δq_x and $\delta\phi_x$ because they introduce an imaginary contribution to the dispersion relation. Substituting the WKB presentation (4.10) into (4.4), (4.5) and introducing, for the low amplitude

case, normalizations $k_1 \rightarrow k \ / \ (6 \ \beta \ \psi_m^2)^{1/2}$, $s_1 \rightarrow s \ / \ 6 \ \beta \ \psi_m^2$ allows us to express the growth rate in the form

$$s_1^2(k_1, x) = \frac{1}{4 \ \omega^2}(\ k_1^2 - 2 \ i \ k_1 \sqrt{6\beta}\psi_m f f_x) \ (\ 6f^2 - 1 - k_1^2 + 3 \ i \ k_1 \sqrt{6\beta}\psi_m f \ f_x) \tag{4.11}$$

where $f(x) = \psi(x)/\psi_m$. At $x = 0$, which corresponds to the peak of the breather, the growth rate, Re s_1, is positive for $k_1^2 < 6f(0)^2 - 1 = 5$. In this case the unstable values of $k_1 < 2.24$ are small and are also out of the range of applicability of WKB approximation, $k_1 >> 1$. Note that this situation is essentially different from the case of the π-mode envelope where solutions of the form (4.10) are valid at any k compatible with the periodic boundary conditions (but still, of course, subject to discreteness limitations).

Small imaginary terms in (4.11) may drive a slow instability with the growth rate, Re $s_1 \simeq (6\beta\psi_m^2)^2$ for values of x where $f_x \neq 0$. To illustrate this situation the imaginary and real parts of s_1 are plotted as a function of k_1, in Fig. 4.1 at the point where f_x is maximum $f_x^{(max)} = (6\beta)^{1/2}\psi_m/2$ and $f = 2^{-1/2}$. This slow growing mode with $s_1 \simeq 0.1$ exists in the range of wavelengths where both WKB and continuous approximations can be valid. These two conditions can be satisfied simultaneously in the case of low amplitude while at high amplitudes it is impossible. Although at short wavelengths the mode is locally unstable there is an additional effect which slows down its growth and may stabilize it. The effect is the convection

of the wave packet in $(x,\ k)$ space due to explicit dependence of s on x and k. This process is described by the equations $\dot{x} = \partial \text{Im } s/\partial k,\ \dot{k} = -\partial \text{Im } s/\partial x$. As it is seen in Fig. 4.1 the value of Im s is large compared to the growth rate, for $k_1 \gtrsim 1.5$ resulting in a fast drift of the packet away from unstable zone to the tail zone where the driving force of instability f_x is small. Furthemore, for $k_1 \leq 1$, where Im s <Re s, we have already seen the WKB approximation fails. The conclusion is that the WKB theory gives no clear evidence that a small amplitude breather is unstable.

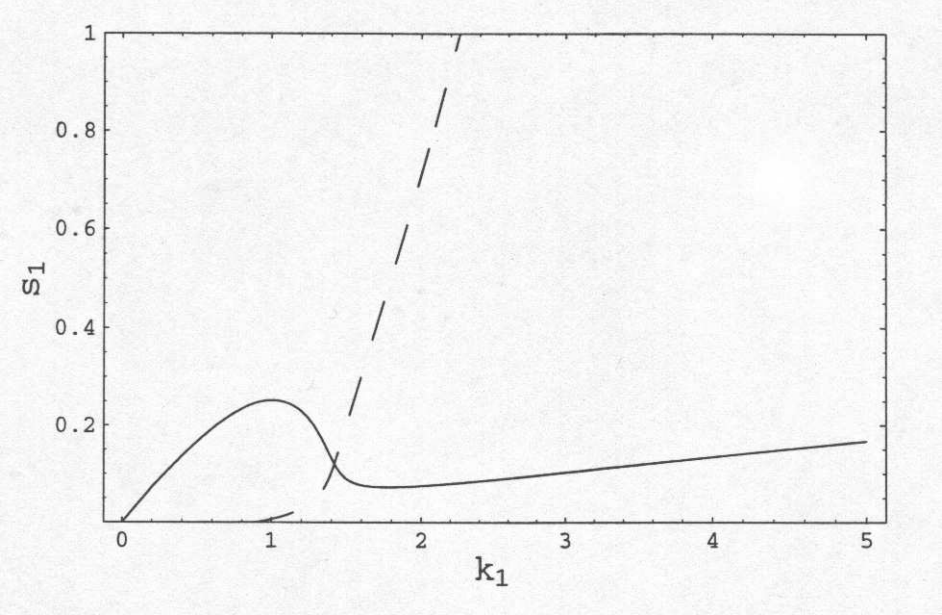

Figure 4.1: Dependence of the normalized growth rate, Re s_1 (solid line) and Im s_1 (dashed line) on the wave number k_1, for the case of a small amplitude breather.

A similar situation occurs in the case of high amplitudes, 9 $\beta\psi_m^2 >> 1$.

Making use of the the analogy with the large amplitude π-mode results in 3.2 one can expect that in this case the typical values of s are of the order of $\omega \simeq \sqrt{6\beta}\psi_m$ so all time derivative terms in (4.2) (4.3) are important. It leads to coupled equations

$$2\ s_2\ \delta q + \psi\ (\ s_2^2 + 2\ i\ k f f_x - (1/2)\ k^2\ f^2\ )\ \delta\phi = 0 \tag{4.12}$$

$$(s_2^2 + 3\ i\ k f f_x + 6f^2 + 3 f f_x + (3/2) f_x^2 - 1 - \ (3/2) k^2 f^2\ )\ \delta q - 2\ s_2\ \psi\ \delta\phi = 0 \tag{4.13}$$

where ω is substituted with its limiting value $\omega \to \sqrt{6\ \beta}\psi_m$ and s is normalized as, $s_2 = s\ /\ (6\ \beta\ \psi_m^2)^{1/2}$ while the wave vector k is not normalized.

Solving equations (4.12),(4.13) for s_2, gives four branches of $s_2\ (x,\ k)$. I will illustrate these results for the most unstable solution. Calculating $s_2\ (x,\ k)$ at the peak of the breather, $x = 0$, yields

$$s_2\ (k) = (1/2)^{1/2} \sqrt{2\ k^2 - 7 + \sqrt{k^4 - 22k^2 + 49}} \tag{4.14}$$

The real and imaginary parts of this solution are shown as a function of k in Fig. 4.2. Although the results indicate a fast instability for a large amplitude breather, the intervals of unstable k are out of the range of applicability of WKB theory or of the envelope approximation. The long wavelength branch of the instability with $k < 1.4$, is not consistent with

the WKB approximation while for the branch with $k > 1.6$ the wavelength of perturbations becomes comparable with the distance between oscillators. Solutions with $k > \pi$ would not be allowed due to the discreteness of the chain. The second derivative term, ψ_{xx}, contributes to the stability at maximum amplitude while destabilazing first derivative terms are small. In the zone where f_x is maximum and, correspondingly, f_{xx} is small, similar to the low amplitude case, these areas can be a source of residual instability, generating waves which then rapidly drift away from the unstable zone.

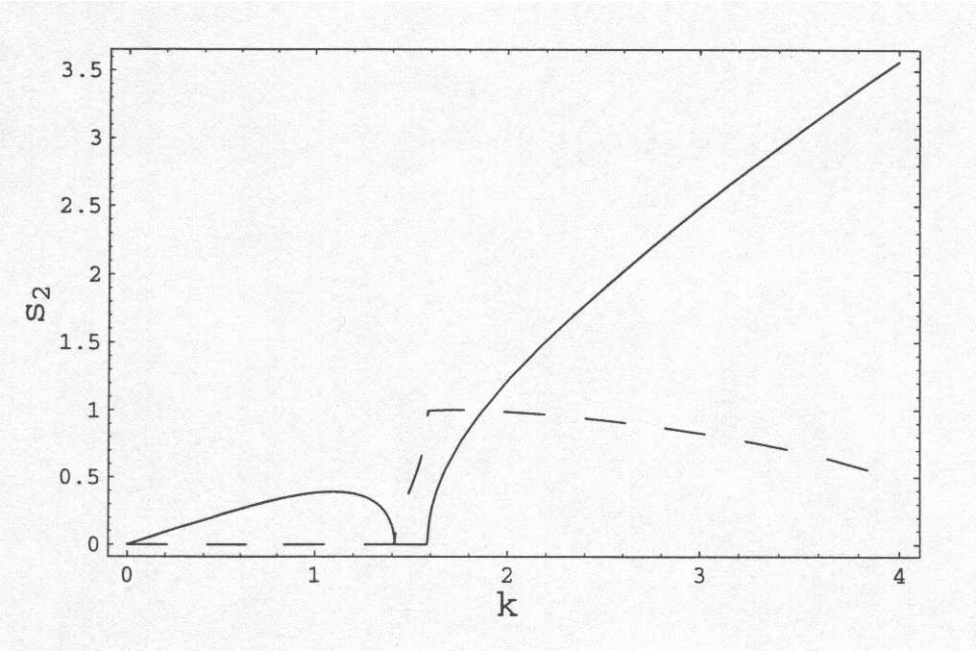

Figure 4.2: Dependence of the normalized growth rate, Re s_2 (solid line) and frequency, Im s_2 (dashed line) on the wave number k around the peak of a large amplitude breather.

One qualitatively concludes that stationary solutions for both low and

high amplitude breathers are such that the width of their profiles is comparable with the most unstable wave lengths (4.8) (4.9), which strongly enhances their stability.

4.2 Numerical Observations Of Relaxation Oscillations And Symmetry Breakup

Since the convective character of the instability and restrictions caused by the conditions of applicability make WKB analysis quite complicated, numerical analysis is important for verifying my qualitative conclusions. The numerical treatment of stability is based on integration of the 128 equations of motion (2.4) for a 128 oscillator chain, with initial conditions $q_i(0) = q_i^{(B)} + \delta q_i,\ p_i(0) = 0$. Functions $q_i^{(B)}$ describe the unperturbed breather profile and they were chosen either from the continuous model in the form of approximation (3.18) for $\psi_m < 1$ or as a breather solution of the discrete FPU model for $\psi_m > 1$. Low and high amplitide initial profiles were centered in the middle of the chain at $x = 64.5$. Large amplitude initial profiles obtained from the discrete FPU problem were treated separetely for symmetric and antisymmetric configurations. In all cases small ($\simeq 10\%$) perturbations with the wave length of the fastest growing mode from (4.8) or (4.9) were added at $t = 0$ to speed up the instability. The time of integration was chosen to be 10 times longer then the inverse growth rate

of the slowest unstable WKB mode considered above which from (4.11) and the normalization scales as $(6\beta\psi_m^2)^{-2}$. Results of these calculations show no significant time variations of the initial profiles over a wide range of amplitudes, $0.1 < \psi_m < 10$. In the case of large amplitudes a rather sudden decay of the symmetric breather was observed after a time which was significantly longer than the times above, so i will not discuss the phenomenon in this chapter. For antisymmetric configurations this effect was not observed. These numerical results confirm stability of the nonlinear envelope solutions (3.16) with $n = 1$. A single breather in an infinite system has a shape similar to envelope solutions (3.16) with $n = 1$, in the case of high amplitudes, $w(n, \psi_m) >> 1$, and would also be expected to be stable. In the low amplitude limit, $w(n, \psi_m) < 1$, the inequality is equivalent to the condition of stability of the π-mode (4.7) such that the breather would also be stable. The envelope solutions (3.16) with higher numbers of n, $n = 2,\ 3....$, consist of n peaks whose profiles are similar to single breathers if $w(n,\ \psi_m) >> 1$ and n is not too high ($n < 25 - 30$). Thus, one can expect stability of the peaks with respect to short wavelength perturbations of their shape. For long wavelength perturbations, a new effect appears when the number of peaks per wavelength is significantly larger than one. In this case perturbations effectively feel the averaged (over x) value of the coefficients in

equations (4.4),(4.5). This results in a long wavelength modulation instability, as described by equation (4.6) for the π-mode, but with avaraged values of f^2. The long wavelength perturbations do not change the shape of individual peaks but lead to the modulation of the peak amplitudes. In this case a modulation instability similar to the instability of the π-mode can be observed in my problem with zero boundary conditions. This long wavelength instability is illustrated in Fig. 4.3 and Fig. 4.4 where the energies of oscillators e_i are plotted for $n = 16$ and two initial conditions, $E = 5$ ($\psi_m = 0.2$) and $E = 20$ ($\psi_m = 0.4$), at $t = 11800$ s and $t = 3500$ s, respectively. Growing perturbations of initially equal amplitudes with the wavelength $\lambda = 64$ and $\lambda = 32$ are well described by the theory of the fastest growing mode (4.6) if averaging is taken into account by reducing their amplitudes to $\psi_m = 0.1$ and $\psi_m = 0.2$. In these cases the nonlinear factor $w(n, \psi_m) = 0.4,\ 0.8$ so the peaks are not well isolated from each other. The global interaction gives rise to a long wavelength modulation instability. In similar calculations at $E = 200$, corresponding to value of $w(n, \psi_m) \simeq 2$, where the peaks are well localized and noninteracting, an instability was not observed. Combining analytical and numerical results one predicts that the nonlinear envelope solutions are stable to the modulational instability in the range of parameters where the nonlinear factor $w(n,\ \psi_m) > 1$.

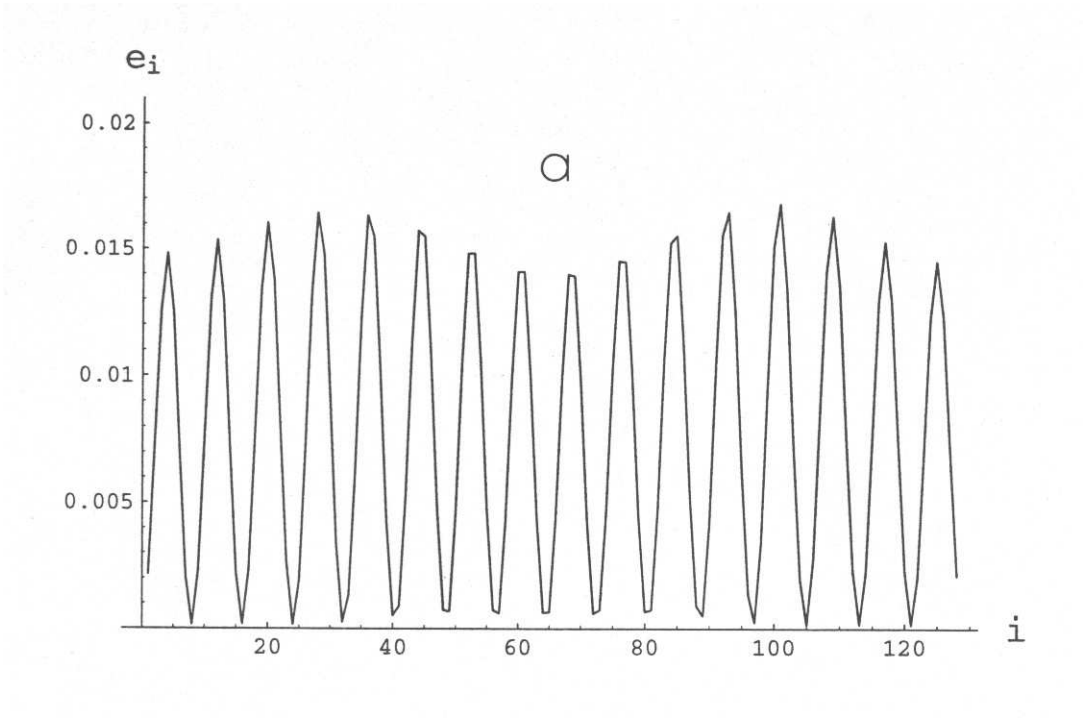

Figure 4.3: Dynamics of the modulational instability of the periodic equilibrium with many peaks ($n \gg 1$). The curves show the profile of the normalized oscillator energies e_i versus i at a time when a long wavelength modulational instability is visible. $E = 5, n = 16, t = 11800$ s; the estimate of the most unstable wavelength, $\lambda_m = 64$, is in a good agreement with the observed wavelength.

Since the initial conditions of much numerical work are taken to be normal modes of the linear problem they are different from nonlinear envelope solutions at the same energy. Normal modes are wider and, therefore, their amplitudes, ψ_i, are less than the amplitudes of corresponding nonlinear solutions, ψ_m. If the value of the difference $\Delta\psi = \psi_m - \psi_i$ is not too large, $\Delta\psi/\psi_m \leq 0.4$, a relaxation takes place in the form of regular oscillations

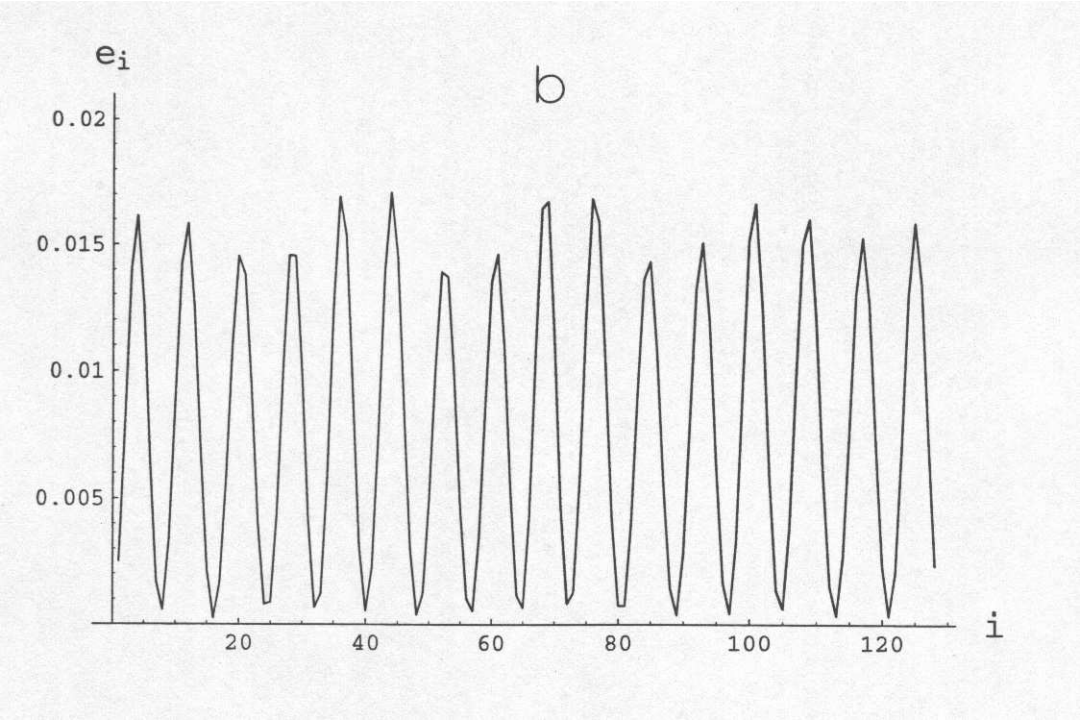

Figure 4.4: Dynamics of the modulational instability of the periodic equilibrium with many peaks ($n \gg 1$). The curves show the profile of the normalized oscillator energies e_i versus i at a time when a long wavelength modulational instability is visible. $E = 20, n = 16, t = 3500$ s; the estimate of the most unstable wavelength, $\lambda_m = 32$, is in a good agreement with the observed wavelengh.

of $\psi(x,t)$ around the equlibrium solution of the same symmetry of amplitude $\Delta\psi$. If $\Delta\psi$ is large, then the relaxation follows another scenario in which $\psi(x,t)$ oscillates around an envelope solution of a different symmetry with higher values of n. This process is more favorable because the equilibrium amplitude of an envelope solution with a higher value of n is lower and, therefore, closer to the initial amplitude at a given energy. A transition from a regular oscillation regime (with conservation of symmetry) to a

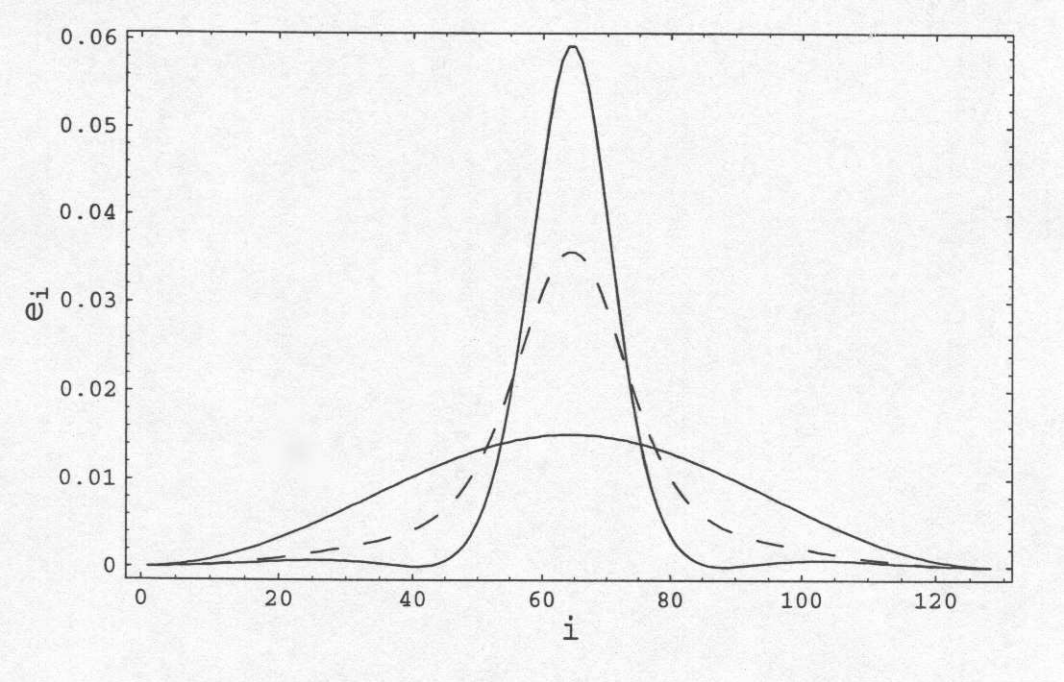

Figure 4.5: Snapshots of oscillator energies e_i versus oscillator number i at successive times, illustrating the dynamics of relaxation from an initial state around the nearest equilibrium state. The dashed line shows the profile of the equlibrium envelope solution with the same initial energy and symmetry. The case of regular oscillations without breakup of symmetry at low energy $E = 0.65, n = 1$; profiles of E_i are shown at $t = 0$ and $t = 1800$ s which correspond to the initial state and maximum of deviation of the envelope function from the initial state.

breakup regime (with change of n) has a threshold depending on the initial amplitude or, equivalently, the energy of the initial state. The transition energy E_{tr} depends on the value of n of an initial normal mode. Numerical results show that the transition energy E_{tr}, starting from a normal mode, increases with n, approximately as n^2, provided n is not too large. This dependence can be explained qualitatively with the use of the nonlinear

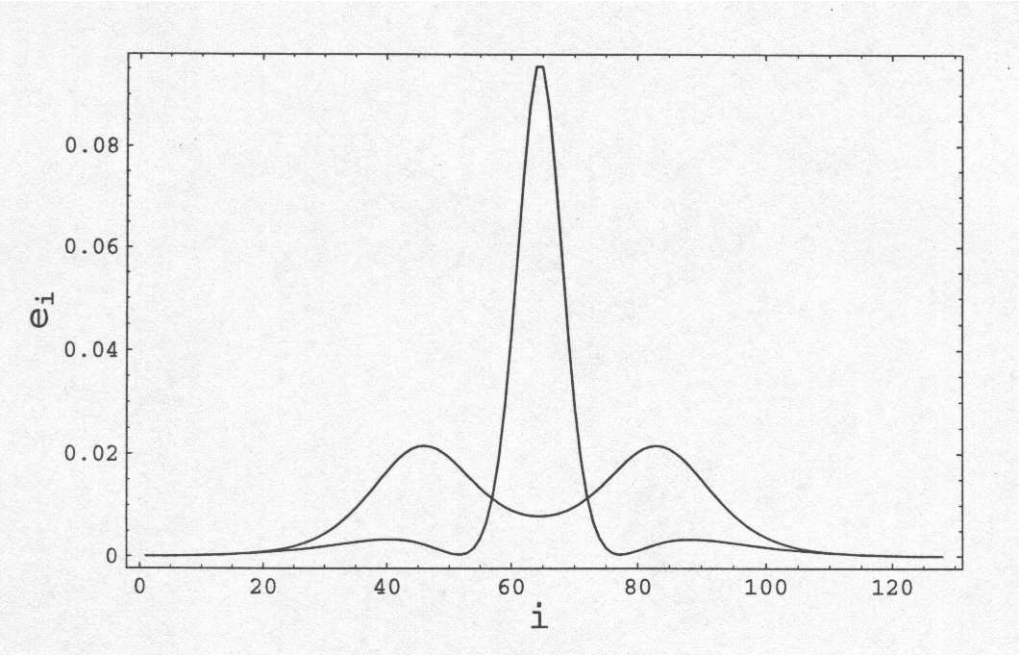

Figure 4.6: Snapshots of oscillator energies e_i versus oscillator number i at successive times, illustrating the dynamics of relaxation from an initial state around the nearest equilibrium state. Illustration of the symmetry breaking at higher energy, $E = 1.29,\ n = 1$; the two distrubutions shown are the profile having initial symmetry at $t = 1000$ s and the transition to the symmetry $n = 2$ at $t = 2000$ s.

parameter w which gives a measure of the difference between strongly nonlinear and almost linear profiles of the envelope solutions. If $w \simeq 1$ the difference is of the order of one also, $\Delta\psi \simeq \psi_m$, which roughly corresponds to the transition from a regular to a breakup regime. From the above it follows that $\psi_{tr} \propto n$ and $E_{tr} \propto n^2$.

These conclusions are illustrated in Fig. 4.5 and Fig. 4.6 where snapshots of numerical results obtained at low energies and $n = 1$, initially, are

given at two times. In Fig. 4.5 the case of regular oscillations with n=1 and $E = 0.65$ is shown. The energy of the individual oscillators are plotted versus i, with the equlibrium profile marked with a dashed line; the period of oscillations is $T = 4000$ s. This initial state is close to the transition to the breakup regime.

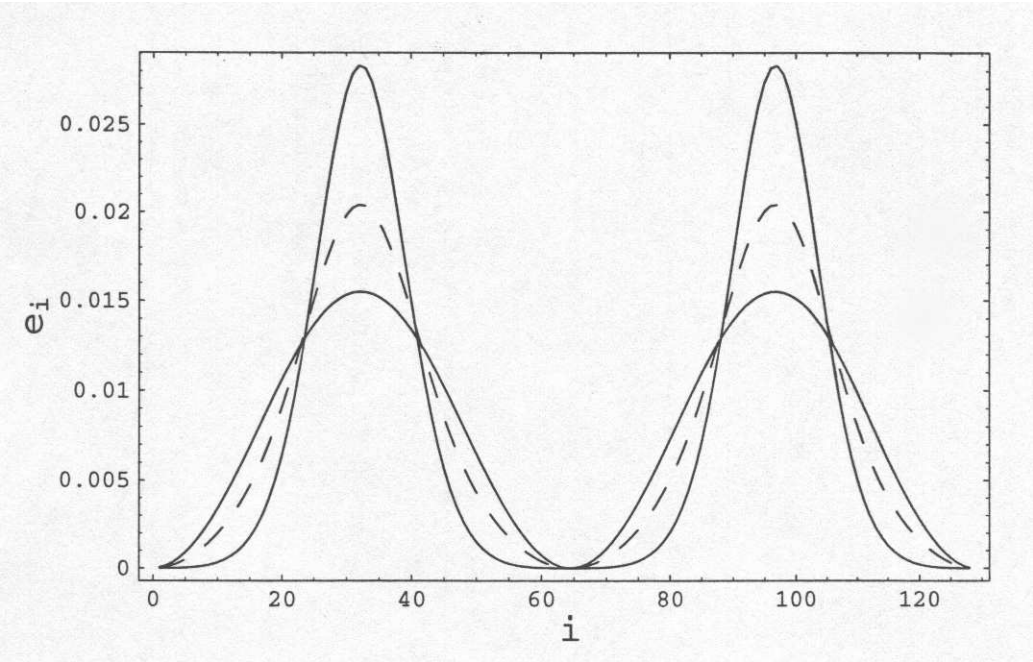

Figure 4.7: The case of the regular oscillations with the initial conditions $E = 1$, $n = 2$ at $t = 0$ and $t = 700$ s. The dashed curve gives the equilibrium profile.

The case of a symmetry breaking oscillation for $n = 1$ but higher energy $E = 1.29$ is shown in Fig. 4.6, where a periodic transition to the symmetry $n = 2$ is observed; the period of oscillation is $T \simeq 4500$ s. A similar situation takes place if the initial normal modes are taken for $n = 2$, as

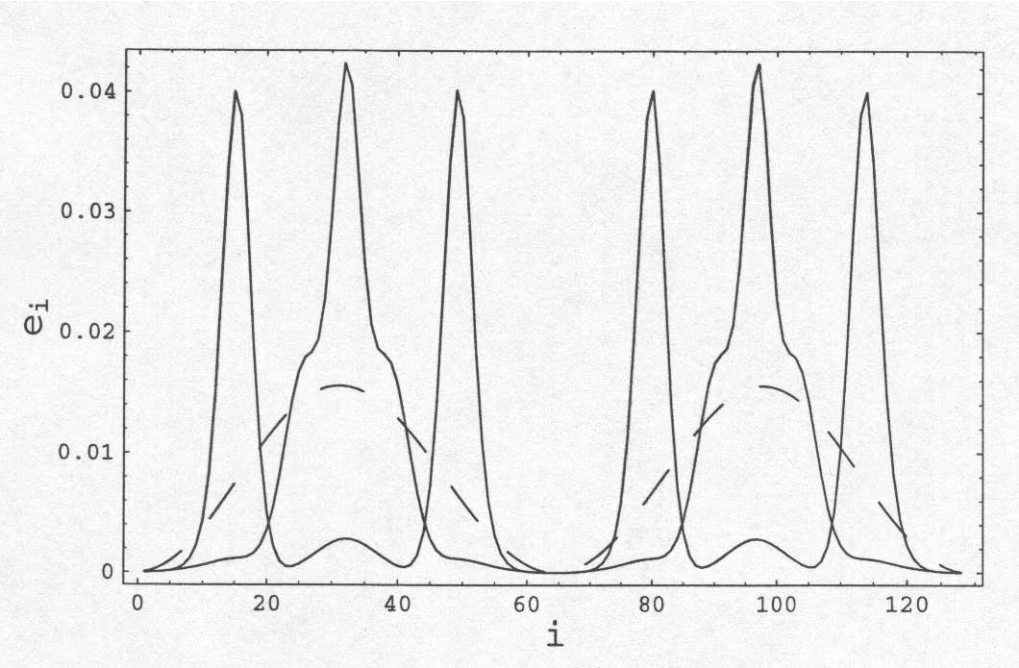

Figure 4.8: The breakup of the initial symmetry $n = 2$ and transition to $n = 4$ in the case of $E = 10$; snapshots correspond to (1) $t = 0$, (2) $t = 200$ s and (3) $t = 1000$ s.

shown in Fig. 4.7 and Fig. 4.8. The regime of regular oscillations is shown in Fig. 4.7 at an energy $E = 1$, with a period of oscillations $T = 1350$ s. For initial energy $E = 10$, symmetry breaking is found as illustrated in Fig. 4.8. The energy E_{tr} at which regular oscillation regime for $n = 2$ makes a transition to the symmetry breaking regime, with $n = 4$ appearing, is about $E_{tr} \simeq 2.6$ which is in a good agreement with the estimate $E_{tr} \propto n^2$.

CHAPTER 5

BREATHER COALESCENCE

After a set of chaotic breathers have been formed, on a short time scale, by a modulational instability or breakup relaxation, the breathers coalesce, on a longer time scale, into a single chaotic breather. This process has been well doccumented, numerically [14, 18, 19], and the process has been studied in more detail in [22]. In fact, the physics is difficult to understand completely, and quantitative comparison of theory, as developed in [22], did not agree with the most detailed numerical results [19]. Our approach will be to first follow the overall calculation program from [22], but extended to include larger amplitude breathers where numerics can be conveniently carried out; then to examine, numerically, the various assumptions that enter into the calculations to see if theoretical estimates can be improved.

5.1 Analytical Estimates

The basic physical notions are that some number of chaotic envelope breathers are formed, related to the fastest growing mode of the modulational instability, initial conditions, and relaxation process. These breathers are moving, in the manner of their low frequency soliton cousins, and therefore collide with one another. Since the breathers are not exact nonlinear solutions to the underlying equations, they interchange energy in the interactions, and also take and lose energy against existing background modes. In a restricted situation, this process has been described theoretically [24], showing that energy is on average transferred from smaller to larger structures. The end result would then be a single large structure. To estimate the time scale for the coalescence, the time scale τ_B is constructed as [22]

$$\tau_B \simeq \frac{l}{v_B} \simeq \frac{1}{n_B \, \sigma \, v_B} \tag{5.1}$$

where v_B is the breather velocity, and the mean free path l is related in the usual way to the density of breathers n_B and the effective cross-section for absorption of colliding breathers σ. The calculation in [22] proceeds from equation (2.15) (without a^4 terms) in the form of Hamiltonian equations for $\Psi(x,t)$ and $\Psi^*(x,t)$ introduced through an amplitude function similar

to (4.1) but in a complex form

$$\psi(x,t) = \frac{1}{2}\left(\Psi(x,t)e^{-i\omega t} + \Psi^*(x,t)e^{i\omega t}\right) \tag{5.2}$$

Droping the terms with the second time derivatives ($\ddot{\Psi} \ll \omega\ \dot{\Psi}$) and using the rotating wave approximation (RWA) yields canonical Hamiltonian equations

$$i\omega\dot{\Psi} = \frac{\delta\mathcal{H}}{\delta\Psi^*}\ , \qquad -i\omega\dot{\Psi}^* = \frac{\delta\mathcal{H}}{\delta\Psi} \tag{5.3}$$

where $\mathcal{H}$ is defined by $\mathcal{H} = \int H dx$ with a Hamiltonian density

$$H\ =\ -\frac{1}{2}\left\{|\Psi_x|^2 - \frac{1}{12}|\Psi_{xx}|^2 - 6\ \beta\ |\Psi|^4 + 6\ \beta\ [|\Psi|^2|\Psi_x|^2 + \frac{1}{4}(\Psi^2\Psi^{*2} + \Psi^2\Psi^{*2})]\right\} \tag{5.4}$$

Equations (5.3) describe slow variation of the envelope and they have the integrals of motion [24]

$$\mathcal{H} = \int H dx\ , \quad \mathcal{P} = -\frac{i}{2}\int(\Psi\Psi_x^* - \Psi^*\Psi_x)\ dx\ , \quad \mathcal{N} = \int|\Psi|^2\ dx \tag{5.5}$$

the energy, momentum and number of quasi-particles, respectively. These results are then used to estimate v_B in (5.1) from the defining quantities in (5.5), which is evaluated in [22] within the approximation of a small amplitude traveling solution, with $N \to \infty$,

$$\Psi(x,t) = \psi_m \frac{\exp(\ ikx - i\Omega t\ )}{\cosh[\sqrt{6\ \beta}\ \psi_m\ (x - v_B\ t)]} \tag{5.6}$$

Expression (5.6) is not an exact solution to (5.3) but satisfies these equations for a reduced Hamiltonian (5.4) in which the second term and last three

terms are droped. In this approximation Ω is the solution to the dispersion relation $\Omega = (3\ \beta/2)\psi_m^2 - k^2/4$ while the wave vector

$$k = -v_B\ (\omega + \Omega)\ \simeq -2\ v_B \tag{5.7}$$

The velocity v_B plays role of the group velocity of the wave packet. Equation (5.7) is equivalent to the usual relationship $v_B = \partial\Omega/\partial k$ and defines k as a function of v_B. The value of v_B by itself is not defined in this approach and is considered as a free parameter. To define the values of v_B an additional argument is used in [22], that due to the interaction of quasi-particles trapped inside the breather quasi-equlibrium values of k and v_B are established, for which the Hamiltonian, $\mathcal{H} = 0$. In analogy with the classical oscillator this statement was called a "virial theorem". Applying this theorem v_B was found to be a linear function of the amplitude

$$v_B\ =\ \sqrt{\beta/2}\ \psi_m \tag{5.8}$$

Note that k postulated in (5.7) is not equal to k_m obtained in (4.8) from the fastest growing mode of the modulational instability. Instead, the reduced form of the Hamiltonian (5.4) gives (5.6) as an exact traveling solution, for which the virial theorem applied to the integral in (5.5) then gives (5.8) and finally from (5.7) i have, $k\ =\ \sqrt{2\beta}\ \psi_m$, which scales like, and is within a relatively small numerical factor of, $k_m\ =\ \sqrt{12\beta}\ \psi_m$. Continuing the argument in [22] the density of breathers n_B, as obtained from the

modulational instability at small amplitude, is

$$n_B \simeq k_{max} \ / \ 2\pi \simeq (\ 3\ \beta\ )^{1/2}\ \psi_m/3 \tag{5.9}$$

and σ is taken from a Born approximation for weak scattering to have proportionality

$$\sigma \propto \left(\int U_{int}\ dx \right)^2 \propto \left(\int \psi_1\ \psi_2\ dx \right)^2 \propto (\ \psi_m^2\ d\ )^2\ \propto\ \psi_m^2 \tag{5.10}$$

Substituting these scalings in (5.1) leads to the scaling $\tau_B\ \propto\ \epsilon_B^{-2}$ where $\epsilon_B\ =\ E_B/N$ is the energy density of the breathers. Recent numerical investigations of the time scale for coalescence, in an energy range that is easily accessible numerically, produced the scaling for the time required to obtain a single CB [19]

$$\tau_B\ \propto\ \epsilon^{-1} \tag{5.11}$$

in contradiction to the small amplitude result (more precisely $\tau_B\ \propto\ E^{-1}$ since N was held constant).

Since numerical treatments mentioned above were mostly done for relatively large energies, the low amplitude scalings (5.8)-(5.10) are not applicable to this case and have to be extended to high amplitudes. I first reconsider the concept of breather velocity for high amplitude. As described above, the reduced equations (5.3) based on the Hamiltonian (5.4) without the second and last three terms, have an exact solution corresponding to the moving breather given in (5.6). However, one can see from (5.6) that the width of

the reduced breather tends to zero when its amplitude increases indefinitely while the full solution in (3.16) for a stationary breather describes a realistic profile which has finite width at any amplitude. This problem raises the questions whether a nonreduced form of Hamiltonian equations (5.3) admits moving breather-like solution or whether the terms, including derivatives, will lead to the solutions with zero v_B. To answer these questions i find, below, an exact solution for a moving breather which satisfies the full a^2 order envelope equation (2.15).

To analyze a moving breather, i will use (4.2), (4.3) and choose solutions in the form $q(x,t) = q(x - u\ t),\ \phi(x,t) = \phi(x - ut)$. Derivatives of these functions with respect to their arguments $\xi = x - ut$, are introduced as q' and ϕ'. Substituting these forms into (4.2), (4.3) and taking into account that $q_t = -u\ q',\ \phi_t = -u\ \phi'$, yields two coupled ordinary differential equations for ϕ and q

$$q\ (1 + u^2 + 3\beta q^2)\ \phi'' + 2q'\ (1 + u^2 + 6\beta q^2)\phi' = 2\ u\ \omega\ q' \tag{5.12}$$

$$(1+u^2)q''+(4-\omega^2)\ q+12\beta q^3+9\beta q(q\ q')'+2\omega u\phi' q-(\phi')^2(1+u^2+6\beta q^2)q=0 \tag{5.13}$$

Equation (5.12) is linear with respect to the first and second derivatives of ϕ and therefore has an exact solution (without singularity at $q = 0$)

$$\phi' = \frac{u\ \omega}{1 + u^2 + 3\beta q^2} \tag{5.14}$$

Subsituting (5.14) in (5.13), multiplaying by q' and integrating over ξ yields a first integral

$$(1+u^2+9\beta q^2)\ q'^2+\left(4-\omega^2+\frac{\omega^2\ u^2}{(1+u^2+3\beta q^2)}\right)\ q^2+6\beta q^4=0 \quad (5.15)$$

where the constant of integration is chosen to be zero to provide zero boundary conditions at infinity. The frequency of the moving breather depends on its amplitude and velocity and can be obtained from (5.15) applied to the point $\xi=0$ where the amplitude $q(\xi)$ reaches its maximum, q_m

$$\omega^2 \ = \ (4+6\beta q_m^2)\left(1+\frac{u^2}{1+3\beta q_m^2}\right) \quad (5.16)$$

Making use of this result, (5.15) can be rewritten in the form of an energy conserving Hamiltonian $h \ = \ q'^2/2+W$ where the effective potential energy W is given by

$$W(q,\ q_m,\ u)=-\frac{3\ \beta\ q^2(q_m^2-q^2)}{(1+9\beta q^2+u^2)(1+3\beta q^2+u^2)}\left[3\beta q^2+1-\frac{u^2}{1+3\beta q_m^2}\right] \quad (5.17)$$

An analysis of the expression in square brackets shows that if the speed of the breather is not too high,

$$u<(\ 1+3\ \beta\ q_m^2\ )^{1/2} \quad (5.18)$$

the effective potential energy is negative at $0\le q\le q_m$ and graphs of $W(q)$ are similar to the curve shown in Fig. 4.1 for the case $C_1=0$. Solving for q' from (5.15) and integrating over ξ yields the breather amplitude $q(\xi)$ which

looks similar to the profile of the standing breather (3.17). If the inequality (5.18) is not satisfied, then the effective potential energy (5.17) becomes positive in some vicinity of $q = 0$, when $(1 + 3\beta q_m^2)^{1/2} < u < 1 + 3\beta q_m^2$; it is positive along the entire interval $0 < q < q_m$, when $1 + 3\beta q_m^2 < u$. In both cases there are no trajectories corresponding to breather-like solutions so equation (5.18) is a necessary and sufficient condition for the existance of a moving breather with arbitrary amplitude.

The new exact solution represents a generalization of the previous solution (5.6), (5.7) to the case of high amplitude breathers. The important result is the dependence of k on x and t described by (5.14). The wave vector $k = \phi'$ has approximately the same value as given by (5.7) in the tail zone of the breather and sharply decreases near the peak dropping down to $2u/(3\beta q_m^2)$. Although the new solution is an exact solution to the full a^2-order equation (2.15), the value of velocity is a free parameter with some weak restriction (5.18). Similar to the calculation of v_B in the small amplitude case (5.8), i make use of the virial theorem based on (5.4) to estimate the effect of large amplitudes on breather velocity. Expressing Ψ and Ψ^* in (5.2) in terms of $q(\xi)$ and $\phi(\xi)$ and substituting into (5.4) gives a Hamiltonian density as a function of $q(\xi)$ and $k(\xi) \equiv \phi'(\xi)$

$$H(q_m,\ u,\ \xi)\ =\ -\frac{1}{2}\ k^2\ q^2\ (\ 1+3\beta q^2\ )\ -\ \frac{1}{2}q'^2(\ 1+9\beta q^2)\ +\ 3\ \beta\ q^4 \quad (5.19)$$

The second term in (5.4) represents the a^4 term $(1/24)\ \psi_{xxxx}$ in (2.15). Since

solutions (5.14) , (5.15) were obtained from a reduced a^2 version of equation (2.15), this term is not included in (5.19) either. It is possible to evaluate the first integral in (5.5) and formulate the virial theorem, $\mathcal{H}(\ q_m\ , u\ )\ =\ 0$, by using the identity

$$\mathcal{H}\ =\ \int H\ d\xi\ \equiv \int H\ dq/q' \tag{5.20}$$

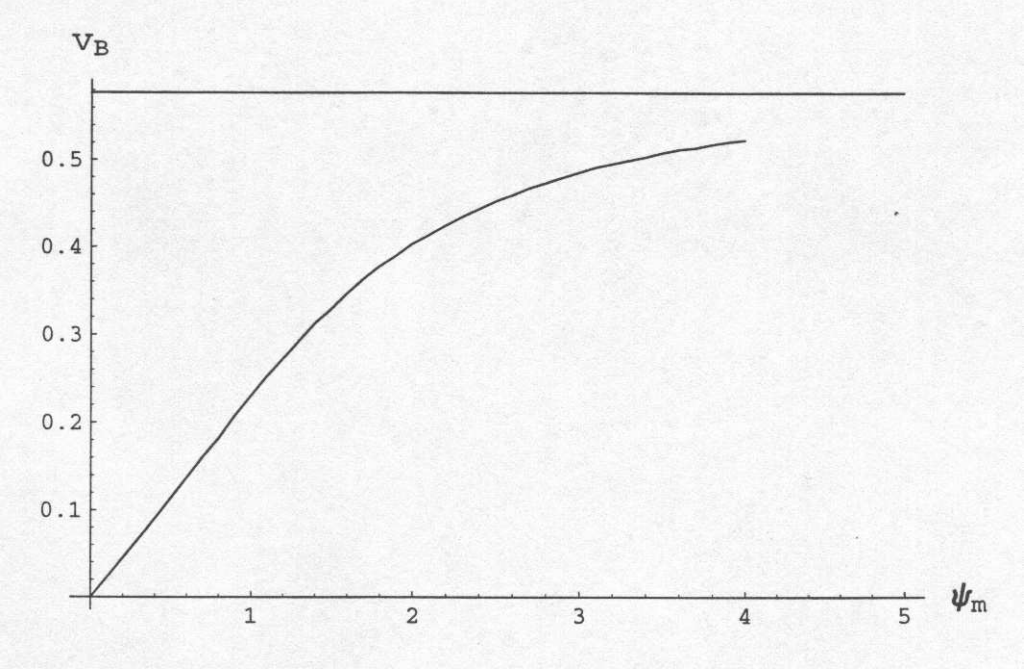

Figure 5.1: Dependence of the breather velocity v_B on its amplitude ψ_m, obtained from the virial theorem. The horizontal line shows asymptotic value of v_B and $\psi_m \to \infty$.

The result after some algebra and a numerical integration over dq, gives the velocity $u \equiv v_B$ as shown in Fig. 5.1. For low amplitude the velocity is

in agreement with (5.8) obtained with the use of (5.6), while for high amplitude we see that v_B becomes asymptotically constant. The remaining quantitives that are required to obtain the scaling (5.1) at high amplitude are obtained in a straightforward way. Taking the wave number of the fastest growing large amplitude mode, from (4.9), we find that $n_B \propto k_{max} = const$, independent of ψ_m, which is consistent with the asymptotic assumption of $v_B = const$ if we admit the above mentioned relationship between k and k_m. From the asymptotic large amplitude expansion of I, in (3.21), we have $\psi_m \propto E^{1/4}$ (with n independent of ψ_m and rougly half the energy in the proto-breathers). Performing the integration in (5.10) for the high amplitude case when the width of the breather $d \simeq 5$ =const, we find

$$\sigma \propto \psi_m^4 \propto E \tag{5.21}$$

Combining the results of v_B and n_B independent of initial E, with (5.21), in (5.1), this gives, at the start of the coalescence, that $\tau_B \propto E^{-1}$ I must, however, follow the time evolution of the caolscence process until a single breather is formed. To do this we note that the time constant is governed by $n_B^{-1}(dn_B/dt) = n_B \sigma v_B$ since n_B decreases as E_B^{-1} and σ increases as E_B, that is, the total energy in the breathers remains nearly constant, then $n_B \sigma$ = const during the coalescence. As found numerically (see below) v_B is relatively constant during this process, and thus we conclude that

$n_B^{-1}(dn_B/dt) = 1/\tau$, a constant, during the decay. Thus the final proportionality for the scaling of coalescence, assuming $E_B \propto E$, is

$$\tau_B \propto E^{-1} \tag{5.22}$$

Comparing (5.11) with (5.22) we see that the asymptotic time scale for coalescence has the same energy scaling as the numerical coalescence time at intermediate energies. This is somewhat surprising, as the numerical result lies between the low energy and high energy asymptotes.

5.2 Numerical Results

To investigate the validity of my various approximations i perform numerical calculations on the discrete oscillator chain. In this way we not only check the approximations that are required to obtain solutions to the nonlinear envelope equations, but also take into account discreteness effects which becomes increasingly important at short wavelengths. I first enquire if the decay is characterized by a single time constant, i.e. if the total number of breathers N_B obeys $(1 \,/\, N_B)(dN_B \,/\, dt) \;=\; 1 \,/\, \tau$, a constant. Taking typical cases of initial energy $E = 20\ ,\ 50$ in mode $\gamma = 120$, i plot $\ln N_B$ vs t, in Fig. 5.2 and Fig. 5.3, respectively. After an initial short period of the modulational instability, the resulting decays are straight line, indicating the constancy of τ.

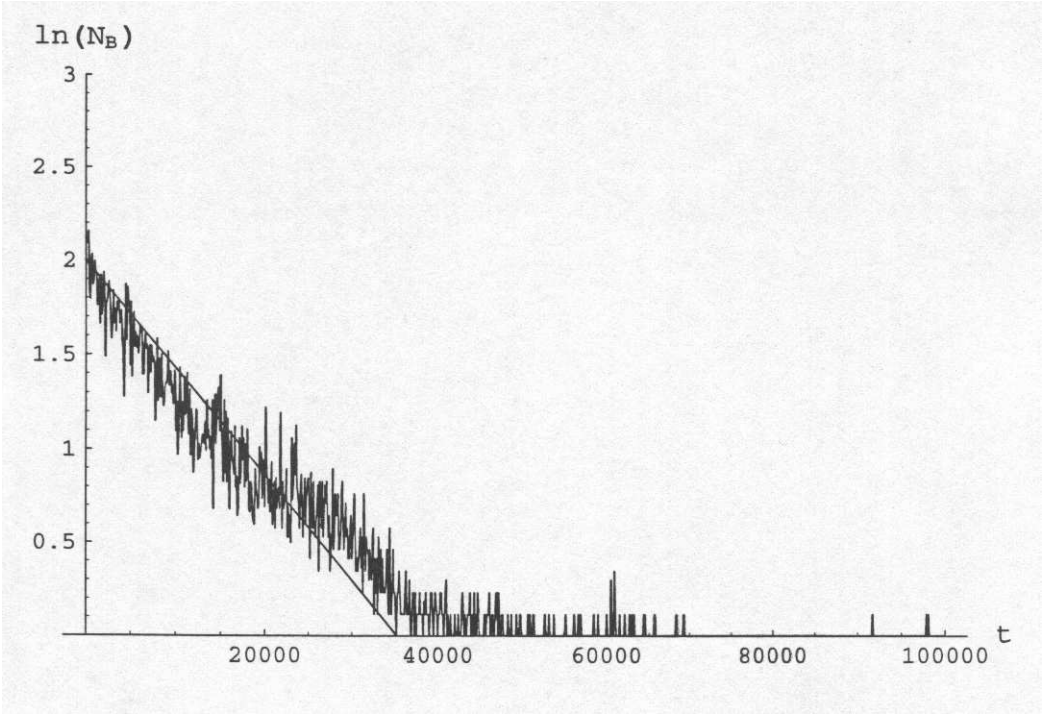

Figure 5.2: Numerical dependences of the number of breathers, $\ln N_B(t)$, versus time. The straight line curves indicate the constancy of the decay time τ during the coalescence from 8-12 breathers to two breathers. The final coalescence to one breather has less statistical accuracy. Initial energy $E = 20,\ n = 9$.

This constancy of τ in the decay process was found to hold well for initial energies $20 \leq E \leq 100$, which is a typical intermediate energy range. At higher energies there is a somewhat longer time for the final coalescence from two breathers to one. Using results like those in Fig. 5.2 and 5.3 the results in Fig. 5.4 are obtained, in the range $20 \leq E \leq 250$. A straight line gives a power law fit to the coalescence time τ_B vs energy, with a best fit giving $\tau_B \ \propto E^{-1.12}$. This is almost the same as the scaling of $\tau_B \propto E^{-1.19}$ in [19] using a somewhat more qualitative criterion for τ_B. Note that τ_B is

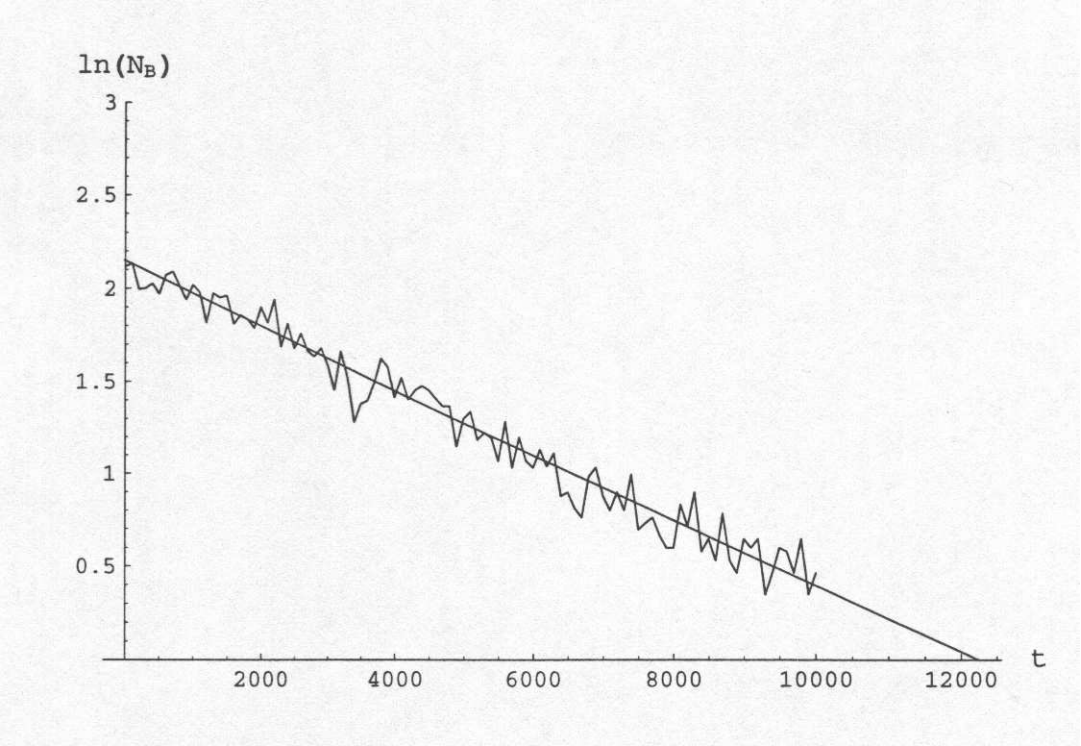

Figure 5.3: Numerical dependences of the number of breathers, $\ln N_B(t)$, versus time. The straight line curves indicate the constancy of the decay time τ during the coalescence from 8-12 breathers to two breathers. The final coalescence to one breather has less statistical accuracy. Initial energy $E = 50,\ n = 9$

not the same as the time constant τ. Typically there are 8-9 initial proto-breathers which coalesce, with the time τ_B being the time necessary for a single chaotic breather to be established. Since in all cases the initial conditions have most of the energy in mode 120, the 8-9 initial peaks tends to be a strong initializing effect for the proto-breathers, as already discussed in Chapter IV.

A further confirmation of our picture of the coalescence process is seen in Fig.5.5 and Fig. 5.6. In Fig. 5.5, for the case of $E = 20$, the motion of the

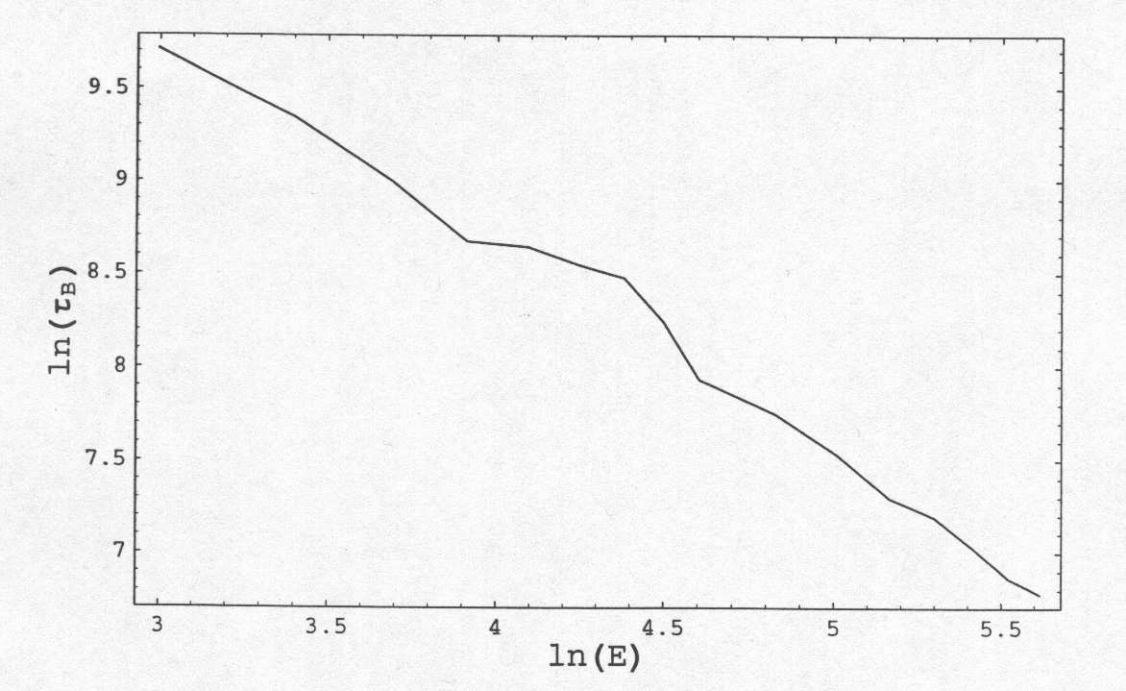

Figure 5.4: Numerical results illustrating the dependence of the decay time $\ln \tau_B$ versus initial energy $\ln E$ obtained from results at various energies as described in Fig. 5.2, 5.3.

largest peak is followed. During the initial stage of proto-breather formation the motion is not well defined as early unstable motion and collisions do not conserve a single proto-breather having the maximum amplitude. At time of 10^4 s the largest breather is established and grows in energy with associated increasing velocity. The velocity

at relatively large amplitude then remains fairly constant in the range 2×10^4 s $\leq t \leq 4 \times 10^4$ s, after which time Fig. 5.2 indicates the existance of a single dominant breather. As seen in Fig. 5.6 the energy of the largest breather is continuing to grow, statistically, during this time. For 4×10^4

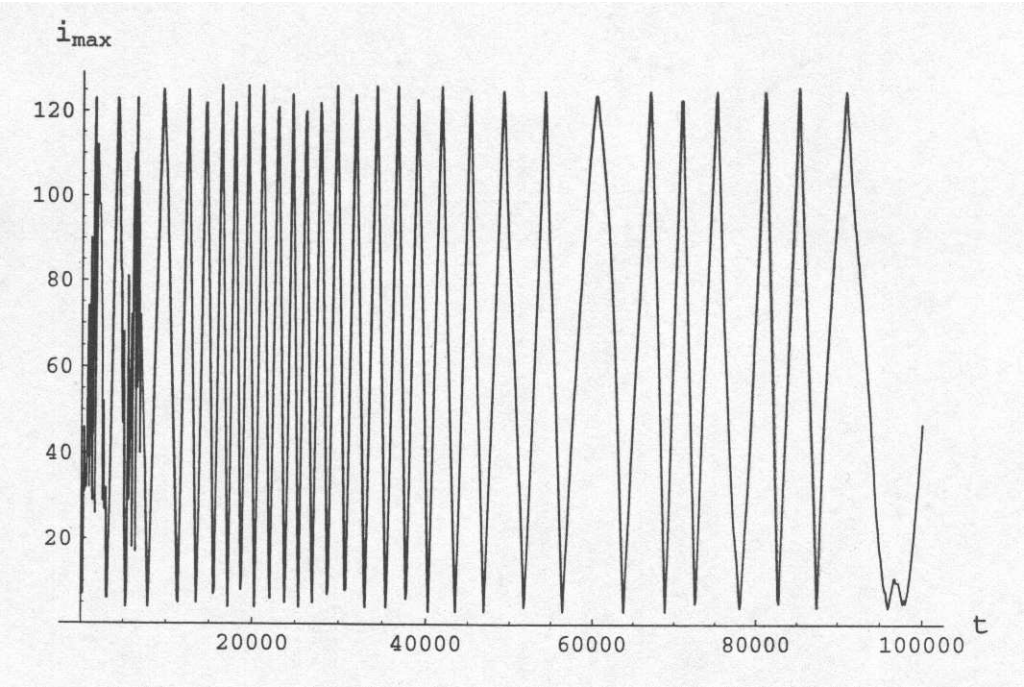

Figure 5.5: Time dependence of the oscillator number i_{max} defined as the position of the oscillator having a maximum energy in comparison with all other oscillators at a given time t. After 10^4 s, when a largest breather is established, it shows the position of that breather.

s $\leq t \leq 10^5$ s, in Fig. 5.5 the single chaotic breather gradually slows down in a somewhat uneven fasion. The explanation of this effect is not within the envelope theory but can be quantitatevely understood by two effects, the well known pinning effect due to the discreteness [18], and the continual interaction with background modes containing a total energy of the order of the breather energy. As seen in Fig. 5.6, during this period the main breather energy is growing slightly. The breather is taking energy from high frequency modes with similar symmetry and giving energy to low frequency

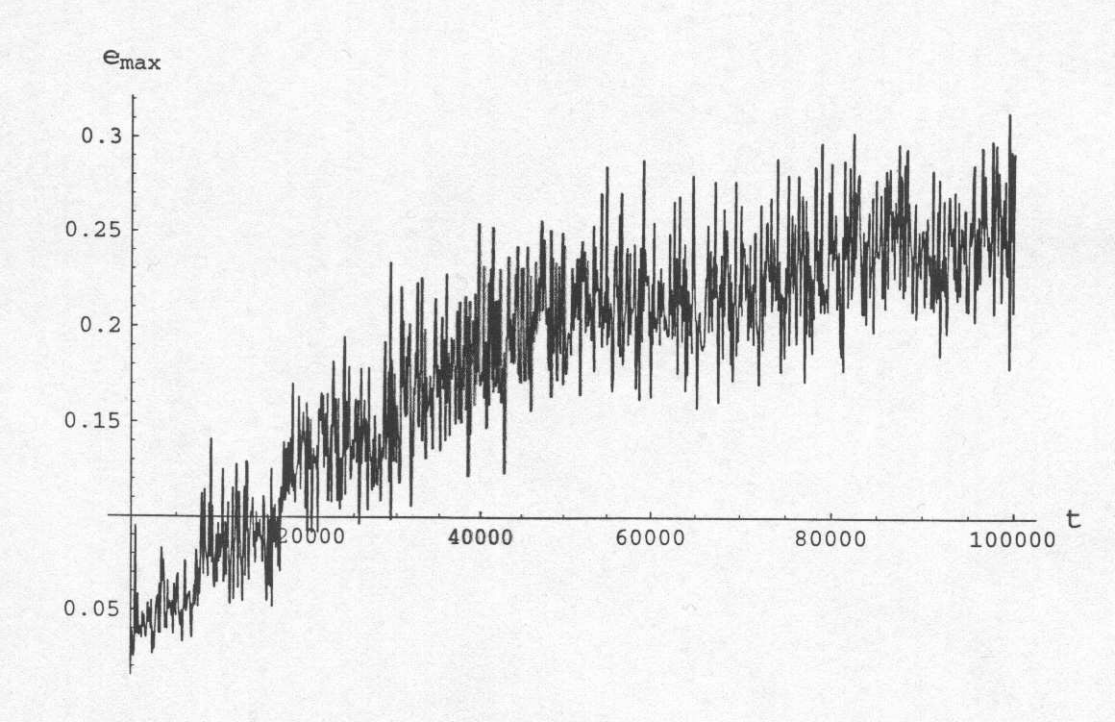

Figure 5.6: Time dependence of the maximum energy $e_{i_{max}}$ of the oscillators described in Fig. 5.5. After the largest breather is established it corresponds to the energy of the oscillator at the peak of the breather.

modes that do not have this symmetry. As described previously [19] and will also be developed in Chapter VI, the breather will decay at longer times, as energy continues to be transferred to low frequency modes and equipartition is approached. Similar dynamics occurs at higher energies, but more rapidly so that the phenomena are not as clearly observed.

CHAPTER 6

BREATHER DECAY

In the usual picture of breather stability, the physical mechanism by which the breather loses stability is that the breather frequency becomes resonant with a linear normal mode [15, 16, 17]. This explanation is not directly applicable to my problem as the breather frequency is higher than the highest mode; e.g. for $E = 50$ ($\beta = 0.1, N = 128$) the CB has a frequency $\omega_B = 2.62$ while the highest mode frequency is $\Omega_h \simeq 2$. However, we know this breather is unstable (a CB), as it must have been formed in the chaotic portion of the Hamiltonian phase space, since it was formed from a few initial modes.Within the usual theory the process then becomes quite subtle, as it depends on the relatively small continuous spectrum of the chaos.

Although the dominant structure is the CB, the mode spectrum, in which the CB can be decomposed, plays an important role. For energy transfer from low frequency to high frequency modes it was shown that the stochasticity developed in low frequency beat oscillations could transfer energy to the high frequency modes via the Arnold diffusion mechanism. The

key requirement for energy transfer on a time scale that is not exponentially slow is that the beat oscillation frequency be as high or higher than the mode (or beat mode) to which the energy is being transfered [9]. In a subsequent paper [20], it was found that the scaling with energy density of the time to reach equipartition can be predicted from that mechanism. The proportionality T_{eq} (low to high) $\propto (E/N)^{-3}$ was predicted and confirmed numerically. In [19] the same formalism has been used to numerically predict the scaling T_{eq} (high to low) $\propto (E/N)^{-2}$. However, the predicted estimate of the time to equipartition was nearly two orders of magnitude shorter than the numerical result. Our current study of breather dynamics has revealed that the method was not applied correctly in [19] when the dominant dynamics is the breather, rather than the normal modes. As stated in [19] "We might expect a significant underestimate of T_{eq} because i am not explicitly taking into account the effect of the CB". In fact, reexamining the beats in the high frequency normal modes indicates that the beat frequency is given by

$$\Omega_B = \omega_B - \Omega_h \tag{6.1}$$

i.e. the difference between the frequency locked to the breather and the background free normal modes. The interaction is, of course, with the high frequency normal modes with the breather symmetry, and so we can take $\Omega_h \simeq 2$. For E=50 with $\omega_B = 2.62$ we find, in Fig. 6.1, the dominant beat

frequency $\Omega_B \simeq 0.6$, which is close to the value $\Omega_B \simeq 0.62$ given by (6.1).

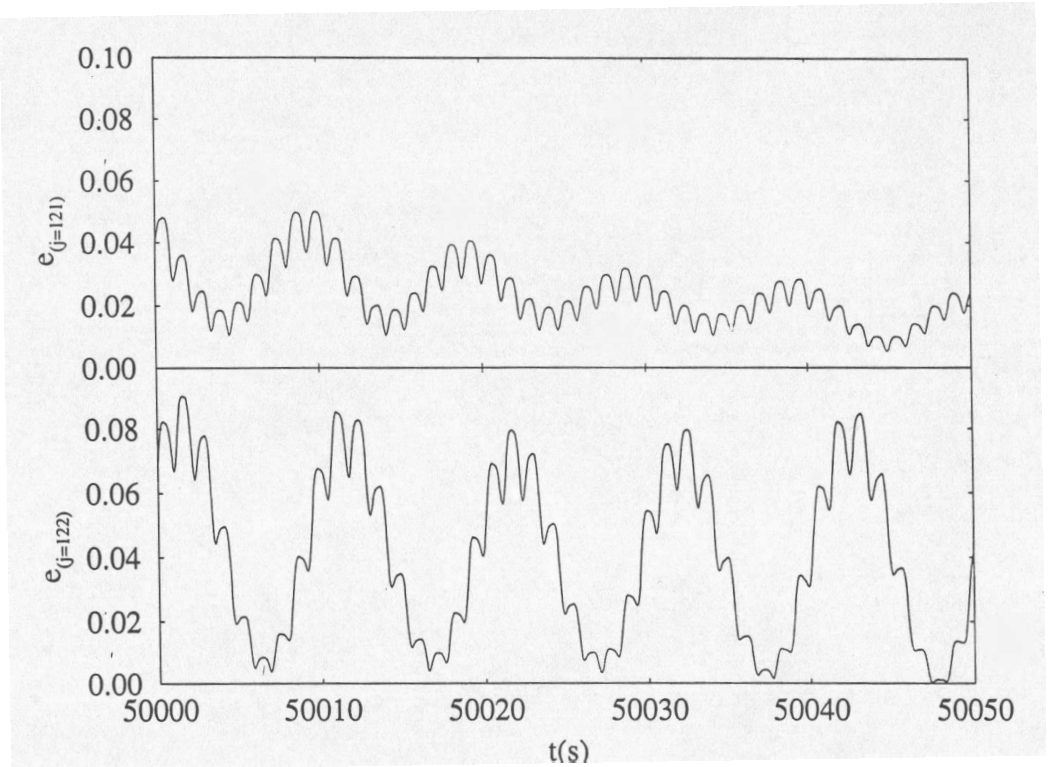

Figure 6.1: Time dependence of the energy of normal mode E_j for $j = 121$ and $j = 122$ during the time interval 50000 s$< t <$ 50050 s when a single chaotic breather is well established ($E = 50,\ n = 9$).

The key assumption in the calculation is to require, for fast Arnold diffusion [9], that

$$\Omega_B \geq \delta\Omega_l \tag{6.2}$$

where $\delta\Omega_l$ is the spread of mode frequencies to which energy can be transferred. For transfer to low-frequency modes

$$\delta\Omega_l = \frac{\pi\delta l}{N} \tag{6.3}$$

where δl is the number of low-frequency modes which are taken to correspond one-to-one with high-frequency modes, δk , $\delta l = \delta k$. To estimate the energy transfer i transform the Hamiltonian (2.3) to normal modes, using (2.8) and (2.9), and then introducing the canonical action-angle variables (I, ϕ) through the transformation $Q_j = \sqrt{2\ I_j\ /\ \Omega_j}\ \cos\phi_j$ and $P_j = \sqrt{2\ I_j\ \Omega_j}\ \sin\phi_j$ we obtain

$$H = \sum_j \Omega_j I_j + \left(\frac{\beta}{8N+8}\right) \sum_{i,j,k,l} G(i,j,k,l)\sqrt{\Omega_i\Omega_j\Omega_k\Omega_l I_i I_j I_k I_l}\ ang(ijkl) \quad (6.4)$$

where $ang(ijkl) \equiv \cos\phi_i \cos\phi_j \cos\phi_k \cos\phi_l$. The coefficients G, as calculated in [3, 4, 5, 6, 7, 8, 9] are

$$G(i,j,k,l) = \sum_P B(i+j+k+l) \quad (6.5)$$

where P represents the eight permutations of sign of j, k and l and the function $B(x)$ takes the value 1 if the argument is zero, -1 if the argument is $\pm 2(N+1)$, and zero otherwise. The selection rule (6.5) follows from the quatric nature of the coupling. Taking the derivative of H with respect to a high frequency angle, we obtain energy transfer from any high frequency mode to all accessible low frequency modes in the form

$$\frac{dE_j}{dt} \simeq C_j\Omega_j \left(\frac{\beta}{N}\right)\ C_l\ \delta l\ E_j\ E_l \quad (6.6)$$

The quantity $C_l\delta l$ is reduced from the quartic sum by the following. The derivative reduces the sum by one index, and the selection rule (6.5) by

a second index. The sum runs over some $(\delta l)^2$ modes. Assuming every quartic term in this sum is typically of the same size and taking the phases to be random, then the effective number of terms is $C_l \delta l$ where C_l was estimated in [20] to be $C_l = 1/4$. The quantity C_j is an efficiency of energy transfer by the Arnold diffusion mechanism, which must be less than $1/2$ (see [1]) and we take $C_j = 1/4$ for definiteness. Note that both factor C_l and C_j were omitted in [19] which contributed to the underestimation of the equipartition time in that thesis. However, my main reworking of that calculation is a new determination of δl from (6.2) and (6.3) using Ω_B from (6.1).

From (3.20) we calculate $E_B(\psi_m)$ and from (3.8) we approximate ω_B, both for $n = 1$ (a single breather). From these results, and using (6.1) we obtain a graph of $\Omega_B(E_B)$ as given in Fig. 6.2 on log-log scale, which we compare with numerical results for Ω_B.

We see that over the main range of energies investigated, we find, approximately, $\Omega_B \propto E_B$ (slope of unity) and furthermore we have an approximate value $\Omega_B \simeq 0.2\beta E_B$. Substituting this, in (6.2), with the equality, and the result in (6.3) we have

$$\delta l = \frac{N}{\pi}\ 0.2\ \beta\ E_B \tag{6.7}$$

Since, within my approximation, $dE_j/E_j = dE_B/E_B$, (6.6) can be rewritten,

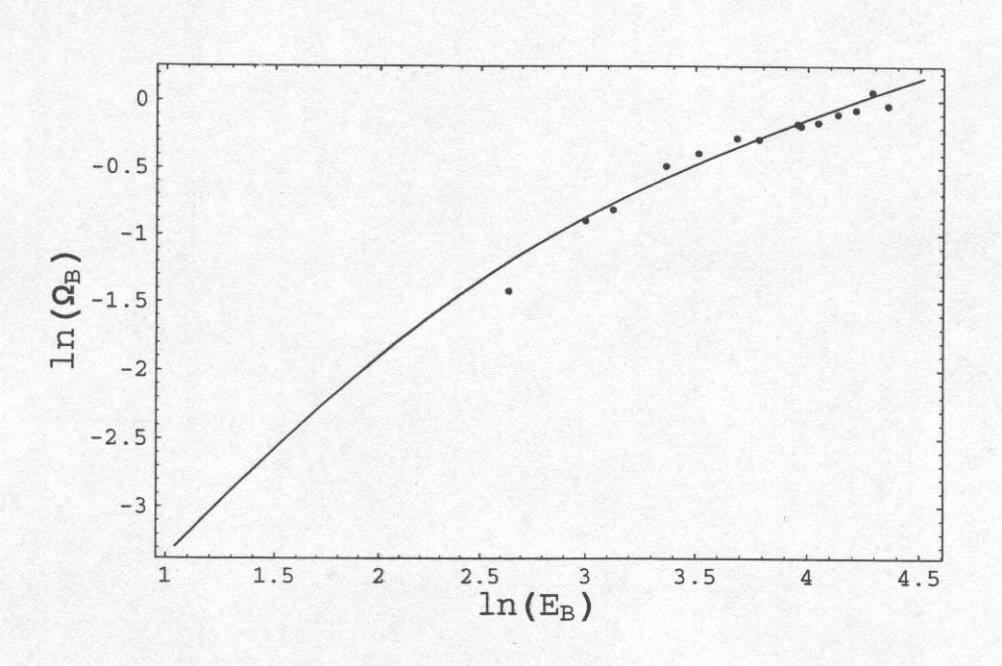

Figure 6.2: Theoretical curve and numerical points illustrate the dependence of beat frequency, $\ln \Omega_B$, on energy, $\ln E_B$, indicating a nearly linear proportionality in the energy range investigated.

$$\frac{dE_B}{E_B^2} = -0.2\ \beta\ C_j\ C_l\ \Omega_j\ \frac{\beta}{N}\ \frac{N}{\pi}\ E_l\ dt \tag{6.8}$$

As in previous work we integrate from E_B(initial) to Ed/N, where $d = n_b^{(init)}$ is the initial number of oscillators in the breather, and E_l from zero to E/N. Using the simplest assumption that $E_l(t) = (t\ /\ T_{eq})\ E/N$, a diffusive process, and taking $d \simeq 5$, we obtain

$$T_{eq} \simeq \frac{80\ \pi}{5}\ \left(\frac{N}{\beta E}\right)^2 \tag{6.9}$$

where i have substituted $C_j = C_l = 1/4$ and $\Omega_j = 2$. I have obtained the

scaling $T_{eq} \propto \epsilon^{-2}$, as found numerically in [19]. For $\beta = 0.1,\ N = 128$ and $E = 50$, $T_{eq} \simeq 3.3 \cdot 10^4$. This is about a factor of five shorter than the time of $T_{eq} \simeq 1.6 \times 10^5$ s reported in [19]

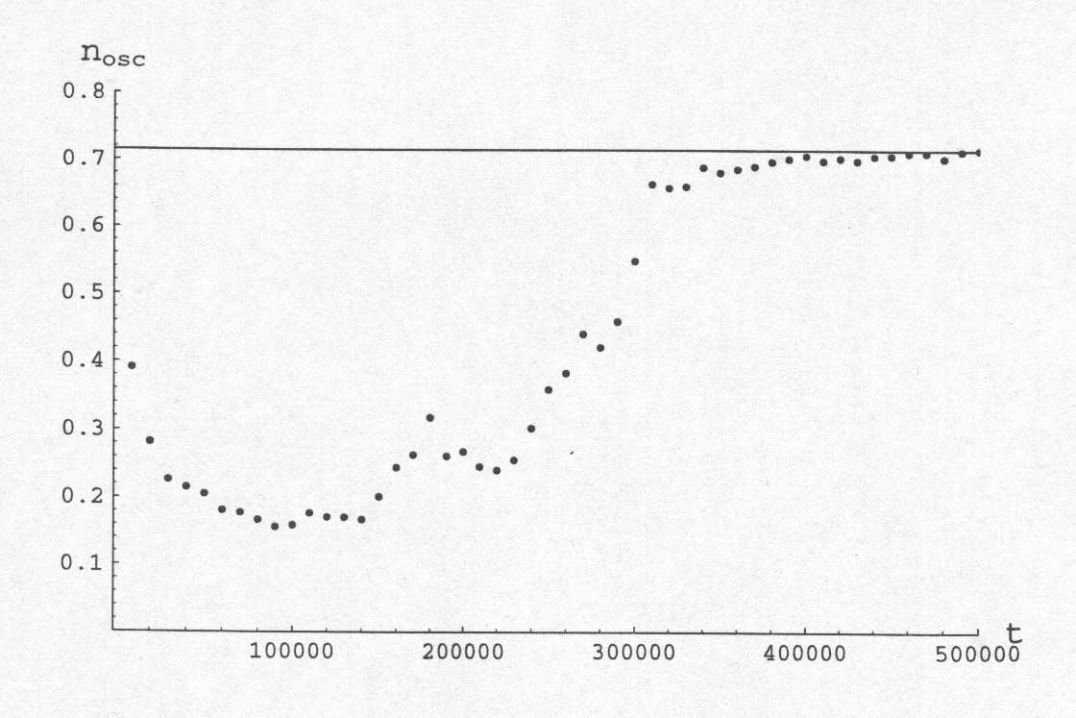

Figure 6.3: Time dependence of $n_{osc}(t)$. The horizontal lines are theoretical asymptotes

There are various arguments to conclude that we have somewhat underestimated the time to equipartition. Particularly, we have not explicitly considerd the complicated process, at intermediate times when the principle CB has been formed but not decayed, and is transfering energy from high frequency modes, that are not part of the breather, to low frequency modes,

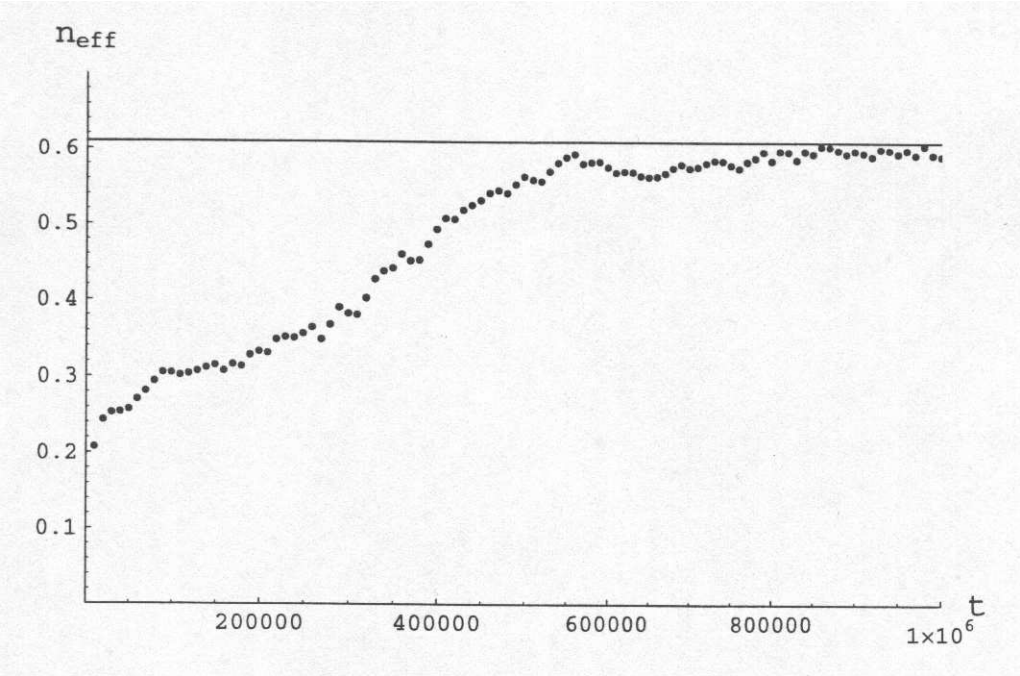

Figure 6.4: Time dependence of $n_{eff}(t)$. The horizontal lines are theoretical asymptotes

using the breather as a catalyst for the transfer. To see these effects i repeat, in a slightly different form from [19], computations of n_{osc} and n_{eff}, given in Fig. 6.3 , 6.4, for $E = 50$, over a time scale in which the various longer time scale dynamical processes can be seen.

The coalescence time period is seen for $t < 2 \times 10^4$ s during which n_{osc} is decreasing rapidly. This is followed by a period ($\Delta t \sim 10^5$ s) in which a single breather is first increasing and then decreasing slowly as energy is transferred from high frequency modes to low frequency modes. Finally there is the more rapid increase in n_{osc}, during which time the

breather energy decays, until equipartition is reached at roughly the time $t \simeq 3 \times 10^5$ s. An average over 10 initial conditions gave the value of $T_{eq} \simeq 1.6 \times 10^5$ s, reported in [19]. The equipartition level at $n_{osc} \simeq 0.7$ and $n_{eff} \simeq 0.6$ can be explained by fluctuations, as described in [12] and [18]. There are some subtlties, not reported in those references, which i describe in Appendix D. I have continued the numerical calculation to $t = 10^7$ s and find the equipartition values to be maintained very closely.

CHAPTER 7

CONCLUSIONS

A chain of equal masses coupled to nearest neighbors by nonlinear springs has a very interesting dynamics, with quite different behavior depending on whether the energy is initially in the low or high frequency part of the allowed spectrum. In particular, the Fermi-Pasta-Ulam (FPU) system, with a quartic hard spring nonlinearity, has been extensively studied. Most of the investigations, both theoretical and numerical, have taken the initial conditions to be in a low frequency linear mode or modes in which neighboring oscillators are mostly in phase. The process by which a resonant interaction of a few low frequency modes can lead to local superperiod beat oscillations that stochastic, transferring energy to high frequency modes by diffusion, has been well studied.

In contrast, if the energy is placed in a high frequency mode or modes, for which neighboring oscillators are primarily out of phase, a more complicated dynamics ensues. High frequency mode initial conditions have phase symmetry of neighboring oscillators close to that of a localized exact breather,

but have a different amplitude profile. The resulting dynamics consists of three stages. First there is an initial stage in which the mode breaks up into a number of breather-like structures. Second, on a slower time scale, these structures coalesce into one large unstable structure, called a chaotic breather (CB). Since a single large CB closely approximates a stable breather, the final decay stage, toward equipartition, can be very slow.

Considerable insight into the behavior of a nonlinear oscillator chain, starting from high frequency initial conditions, can be obtained by introducing an envelope function for the displacements of the oscillators. The initial conditions for the envelope only contain significant long wave length perturbations. For the envelope function an expansion is then possible to obtain a nonlinear partial differential equation (PDE) which approximates the behavior of the discrete system. Low-order expansions of this type produce PDEs that have integrable solutions in the form of envelope solutions, analogous to the solutions produced from low-frequency initial conditions. However, initial conditions chosen to be close to a high frequency mode of the linear system, give envelope profiles far from those of breathers.

For the quartic FPU chain with fixed ends i have obtained PDE's for the envelope function of the discrete chain, Taylor expanded to fourth order in the separation between oscillators. The resulting equations have been solved to obtain nonlinear periodic structures similar to isolated breather

solutions. The relationship between structure amplitude and width have been obtained, showing that the width decreases with the amplitude at low amplitude and becomes asymptotically constant at high amplitude, analogous to the behavior of isolated stable breathers.

I have examined the stability of the nonlinear structures to perturbations. The analysis becomes complcated due to spatial variations. However a local analysis of the growth rate of the modulational instability indicates that, for wavelengths which satisfy the Taylor expansion, the perturbations convect away faster than they grow, thus effectively stabilizing the modes. This result is in a contrast to the highest mode with periodic boundary conditions (π-mode), which has a uniform amplitude envelope solution which becomes unstable at a particular energy. For energies sufficiently low that a normal mode initial condition is relatively close to the equilibrium, a linear stability analysis is reasonable. In this case the most unstable uniform initial distribution is below the stability boundary, and therefore stable. The normal mode initial conditions at intermediate or high energies are far from the nonlinear equilibria with the same symmetry , and therefore subject to large amplitude relaxation oscillations. Underlying stability considerations, and the proximity of equilibria with other symmetries, lead to breakup of the initial symmetry, if the energy is sufficiently high. The number of protobreather peaks established in this process, starting from a symmetry of a

few initial peaks, is usually larger than the initial number of peaks, but depends on the energy. The particular case studied in [19], and also in this thesis, of $n = 9$ ($\gamma = 120$) led to resultsof 8-12 proto-breathers in the energy range $20 < E < 200$. This result can be qualitatively understood by a balance between a minimizing of the oscillation amplitude within a peak with a tendency for the peaks to remain isolated. The one situation in which the modulational instability theory can be applied to spatially varying equilibrium profiles is for an initial n relatively large but at not too high an energy. In this case the instability wavelength is long enough that the forces driving it can be averaged over a number of peaks. The uniform amplitude instability theory predicts the k-value $k_m \propto \sqrt{\beta < \psi^2(x) >}$ and the growth rate, $s_m \propto \beta < \psi^2(x) >$ where the spatial average over x replaces ψ_m^2, as described in Chapter IV. At high energies $k_m = 1.23$ such that the predicted wavelength for maximum growth is comparable to the breather width and therefore the averaging is not valid.

After a set of quasi-stable proto-breathers are formed, they move slowly in random directions, colliding with one another. In this process the proto-breathers can pass through each other or be reflected, losing or gaining energy in the interaction. On average the large structures absorb energy from the smaller ones, as expected from general theoretical considerations.

The time constant for coalescence into a single chaotic breather (CB) was estimated in [22] from the relation $\tau_B \simeq (N_B\ \sigma v_B)^{-1}$ where N_B is the breather number, σ a collision cross-section for absorption, and v_B a characteristic velocity. Using the procedure, extended to higher energies, i obtained reasonable agreement with the numerical scalings of$\tau_B \propto E^{-1}$. Furthemore i demonstrated that $\tau \equiv N_B(dN_B/dt)^{-1}$ is essentially constant during the decay, such that $\tau_B \propto \tau$, in agreement with my theoretical prediction.

To calculate the scaling and the time T_{eq} for the CB decay, to obtain energy equipartition, i adopted a theory developed for stochastic transfer of energy from low-frequency to high-frequency modes by means of chaotic beat oscillations [20]. For transfer in the reverse direction the relevant beat frequency is given by the relation $\Omega_B = \omega_B - \Omega_h$, where ω_B is the breather frequency, $\omega_B^2 \simeq 4 + 6\beta\psi_m^2$, and $\Omega_h \simeq 2$ for a high frequency mode. Using this scaling and the theoretical relation between E and ψ_m, i predict that $T_{eq} \propto \epsilon^{-2}$, as found numerically for varying E and constant N, and furthermore were able to calculate a value of T_{eq} for $E = 50$ to within a factor of five of the numerical value. I could also qualitatively explain the rather longer times found numerically. The numerical equipartition values of $n_{osc} \simeq 0.7$ and $n_{eff} \simeq 0.6$, for oscillators and modes, respectively, agreed with the analytic values and furthermore remain quite constant for numerical integration times a factor of 10 longer than required to first obtain

the equipartition values.

I conclude that the general process, by which the energy initially placed in a high frequency mode reaches equipartition among modes, is understood. The time-scales for the longer-time processes can also be calculated , approximately. The physical mechanism explains why the transfer of energy from high frequency to low frequency modes is slower than the reverse transfer. It also sheds light on the interesting question of whether nonlinear chaotic process will tend to create coherent localized structures. The answer, at least within the context of this study, is that such localized structures can form transiently , but the ultimate most-probable state is that of equipartition among the system modes. I do not address the question of whether long-time Poincare recurrances can occur in such nondissipative systems, but any such recurrances in high-dimensional systems would be beyond any numerical investigation time.

REFERENCES

[1] A.J.Lichtenberg and M.A.Lieberman, Regular and Chaotic Dynamics, Springer Verlag, Berlin (1992)

[2] E.Fermi, J.Pasta, S.Ulam and M.Tsingtou, reprinted in: The Many-Body Problem, D.C.Mattis ed., World Scientific, Singapore (1993)

[3] J.Ford, Journal of Mathematical Physics 2, 387 (1961)

[4] F.M.Izrailev, and B.V.Chirikov, Dokl. Akad. Nauk SSSR 57, 166 (1966) [Sov. Phys.-Dokl. 11, 30 (1966)]

[5] P.Bocchieri, A.Scotti, B.Bearzi and A.Loinger, Phys. Rev. A 2 2013 (1970)

[6] R.Livi, M.Pettini, S.Ruffo, M.Sparpaglione and A.Vulpiani, Phys.Rev. A 31, 1039 (1985)

[7] M.Pettini and M.Landolfi, Phys. Rev. A 41, 768 (1990)

[8] H.Kantz, R.Livi and S.Ruffo, J. Stat. Phys. 76, 627 (1994)

[9] J.DeLuca, A.J.Lichtenberg, and M.A.Lieberman, Chaos 5, 283 (1995)

[10] J.DeLuca, A.J.Lichtenberg and S.Ruffo, Phys. Rev. E 51, 2877 (1995)

[11] C.F.Driscoll and T.M.O'Neil, Phys. Rev. Lett. 37, 69 (1976); Rocky Mt. J.Math. 8, 211 (1978)

[12] C.G.Goedde, A.J.Lichtenberg, and M.A.Lieberman, Physica D 57, 200 (1992).

[13] M.C.Forrest, C.G.Goedde and A.Sinha, Phys. Rev. Lett. 68 2722 (1992)

[14] V.M.Burlakov, S.A.Kiselev and V.I.Rupasov, Phys. Lett. A 147, 130, (1990); V.M.Burlakov and S.A.Kiselev, Sov. Phys. JETP 72 854 (1991)

[15] O.Bang and M.Peyrard, Phys. Rev. E 53, 4143 (1996)

[16] J.L.Marin, and S.Aubry, Nonlinearity 9, 1501 (1996); Physics D 119, 163 (1998)

[17] T.Cretegny, S.Aubry and S.Flach, Physica D 119, 73 (1998)

[18] T.Cretegny, T.Dauxois, S.Ruffo and A.Torcini, Physica D 121, 109 (1998)

[19] K.Ullman, A.J.Lichtenberg and G.Corso, Phys. Rev. E 61, 2471 (2000)

[20] J.DeLuca, A.J.Lichtenberg and S.Ruffo, Phys. Rev. E 60, 3781 (1999)

[21] Yu.A.Kosevich, Phys. Rev. B 47, 3138 (1993); Phys. Rev. B 48, 3580 (1993)

[22] Yu.A.Kosevich and S.Lepri, Phys. Rev. B 61, 299, (2000)

[23] T.Dauxois, S.Ruffo and A.Torchini, Phys. Rev. E 56, R6229 (1997)

[24] A.I.D'yachenko, V.E.Zakharov, A.N.Pushkarev, V.E.Shvets and V.V.Yan'kov, Sov. Phys. JETP, 69, 1144 (1989)

APPENDIX A

ASYMPTOTIC EXPANSION OF $I(Y)$

Expressing (3.11) in terms of $y = 6\beta\psi_m^2$ and making straightforward transformations yields

$$I(r,y) = \frac{2}{\pi}\int_0^{\pi/2} \frac{d\alpha}{\sqrt{\sin^2\alpha \ + \ r^2}} \ + \ \frac{18y}{\pi}\int_0^{\pi/2} \frac{d\alpha \ \sin^2\alpha}{\sqrt{\sin^2\alpha \ + \ r^2}} \frac{1}{(\sqrt{1+9y\sin^2\alpha} \ + \ 1)} \tag{A.1}$$

Applying an asymptotic expansion at $r \to 0$ for the first integral and putting $r = 0$ in the second one gives

$$I(r,y) \ = \ \frac{2}{\pi} \ \ln \ \frac{4}{r} \ + \ \frac{18 \ y}{\pi}\int_0^{\pi/2} \frac{d\alpha \ \sin\alpha}{\sqrt{1+9y\sin^2\alpha} \ + \ 1} \tag{A.2}$$

After a few subsitutions the integral is calculated analytically yielding asymptotic expression for $I(r,y)$

$$I(r,y) \ = \ \frac{2}{\pi} \ \ln \ \frac{4}{r} \ + \ \frac{6\sqrt{y}}{\pi}\arcsin\sqrt{\frac{9y}{9y+1}} \ - \ \frac{1}{\pi}\ln(9y+1) \tag{A.3}$$

APPENDIX B

ENERGY OF THE NONLINEAR ENVELOPE SOLUTIONS

Expression (2.3) for energy H can be rewritten in terms of envelope function $\psi_i(t) = (-1)^i \; q_i(t)$:

$$H = \sum_{i=0}^{N+1} \left[\frac{1}{2}\dot{\psi_i}^{\,2} + \psi_i^2 + \psi_{i+1}\psi_i + \frac{\beta}{2}(\psi_i^4 + 3\,\psi_{i+1}^2\psi_i^2 + 2\,\psi_{i+1}^3\,\psi_i + 2\,\psi_{i+1}\,\psi_i^3) \right] \tag{B.1}$$

Substituting Taylor's expansion (2.14) and collecting terms proportional to different powers of a yields:

$$H = \frac{1}{a}\int_0^{(N+1)a} dx \; \{ \frac{1}{2}\,\psi_t^2 + 2\psi^2 + 4\,\beta\,\psi^4 + a\,(\psi\psi_x + 7\,\beta\,\psi^3\psi_x) + \frac{a^2}{2}\,[\,\psi\psi_{xx} + \beta\,(7\,\psi^3\psi_{xx} + 9\,\psi^2\psi_x^2)] + \frac{a^3}{6}[\psi\,\psi_{xxx} + \beta\,(\,6\,\psi\,\psi_x^3 + 7\,\psi^3\psi_{xxx} + 27\,\psi^2\,\psi_x\,\psi_{xx})] + \frac{a^4}{24}\,[\,\psi\,\psi_{xxxx} + \beta\,(7\,\psi^3\,\psi_{xxxx} + 27\,\psi^2\psi_{xx}^2 + 36\,\psi\,\psi_x^2\,\psi_{xx} + 36\,\psi^2\,\psi_x\,\psi_{xxx})]\} \tag{B.2}$$

Introducing the dimensionless variable $x \to x/a$, performing an integration by parts and taking into account boundary conditions $\psi(0,t) = \psi(N +$

$1,t) = 0$ yields

$$H = \frac{1}{12}[\psi_x^2(0) - \psi_x^2(N+1)] + \frac{1}{24}[\psi_x\psi_{xx}(0) - \psi_x\psi_{xx}(N+1)] + \\ + \int_0^{N+1} dx \{ \frac{1}{2}\ \psi_t^2 \ + \ 2\psi^2 + 4\ \beta\ \psi^4 - \frac{1}{2}\psi_x^2 - 6\beta\ \psi^2\psi_x^2 + \\ + \frac{1}{24}\ [\ \psi_{xx}^2 + \beta\ (12\ \psi^2\psi_{xx}^2 + 6\ \psi\ \psi_x^2\ \psi_{xx})]\} \qquad (B.3)$$

Applying this expression for the harmonic dependence $\psi(x,t) = \psi(x)\cos\omega t$ and averaging over time in accordance with $\cos^2\omega t = 1/2, \quad \cos^4\omega t = 3/8$ gives

$$H = \frac{1}{24}[\psi_x^2(0) - \psi_x^2(N+1)] + \frac{1}{48}[\psi_x\psi_{xx}(0) - \psi_x\psi_{xx}(N+1)] + \\ \frac{1}{4}\int_0^{N+1} dx \{ \omega^2\psi^2 + \ 4\psi^2 - \psi_x^2 + 6\ \beta\ \psi^4 - 9\beta\ \psi^2\psi_x^2 + \\ + \frac{1}{24}\ [2\ \psi_{xx}^2 + \beta\ (18\ \psi^2\psi_{xx}^2 + 9\ \psi\ \psi_x^2\ \psi_{xx})]\} \qquad (B.4)$$

Substituting (3.16) into (B.4) and ignoring terms which originate from the forth order a^4 terms yields equation (3.20) for the energy of the system. For the case of a strongly nonlinear envelope, putting, $r = 0$, allows us to express energy as

$$E = (2\ n\ \psi_m/\sqrt{6\beta}\ )Z(y) \qquad (B.5)$$

where $y = \beta\psi_m^2$ and

$$Z(y) = \int_0^{\pi/2} d\alpha\ (1\ +\ 9\ \beta\ \psi_m^2\ \sin^2\alpha)^{1/2}((3\ \beta\ \psi_m^2 \sin^3\alpha\ +\ 2\ \sin\alpha\ ) \qquad (B.6)$$

The integral $Z(y)$ is calculated exactly, giving

$$Z(y) = \frac{25}{24} + \frac{9}{8}\, y + (23 + 234\, y + 243\, y^2)\, \frac{\arctan(\, 3\, \sqrt{y})}{72\, \sqrt{y}} \qquad (B.7)$$

APPENDIX C

CONDITIONS OF VALIDITY OF $\mathbf{a^2}$-APPROXIMATION

Analytic results in Chapter III are based on the reduced form (3.5) in which all terms proportional to a^4 and higher powers of a are dropped. I now discuss the validity of this approach by examining (3.1) which includes all terms of order a^4. Solving (3.1) numerically and comparing results with the corresponding solutions to (3.5) allows us to find the domain of validity of (3.5) and, more generally, of the continuous approximation.

Comparing linear terms one concludes that the reduced linear form of (3.1) has one additional term, $(1/12)\psi_{xxxx}$, with respect to linear equation (3.2). Its solutions with zero boundary conditions at $x = 0$ and $x = N + 1$ have the same form as (3.3) but the eigenfrequency ω is higher than given by (3.4),

$$\omega^2 \;=\; 4 - q_n^2 + \; q_n^4 \;/\; 12, \qquad\qquad q_n = \pi \; n/(N+1) \qquad\qquad (C.1)$$

due to the factor q_n^4 / 12 which corresponds to the next term in Taylor's expansion with $\pi n/(N+1) \ll 1$ ($j = \gamma = N + 1 - n$).

Despite the complexity of the nonlinear equation (3.1) it has an exact

first integral which can be obtained by myltiplying (15) by ψ_x and integrating over x. The result of the calculation gives

$$(-\omega^2+4)\ \psi^2+\ (1+9\ \beta\ \psi^2)\ ({\psi_x}^2\ +\ (1/6)\ \psi_x\ \psi_{xxx}-\ (1/12)\ {\psi_{xx}}^2)+$$

$$+\beta\ (6\ \psi^4+3\ \psi\ {\psi_x}^2\ \psi_{xx}+(3/8)\ {\psi_x}^4)=\ C_1 \qquad (C.2)$$

Choosing, $C_1 = 0$, we select the class of localized, breather-like solutions for a chain of oscillators that is infinitively long ($N \to \infty$). The breather envelope function has one maximum, ψ_m, which is taken to be in the middle of the chain at $x = 0$, which is the origin of the new reference frame, and $\psi \to 0$ at $x \to \pm\infty$. Applying (C.2) at $x = 0$, with $\psi_x(0) = 0,\ \psi_{xx}(0) < 0$, yields an equation for the eigenfrequency

$$\omega^2\ =\ 4+6\ \beta\ \psi_m^2\ -\ (1/12)\ (1\ +\ 9\ \beta\ {\psi_m}^2)\ f_{xx}(0)^2 \qquad (C.3)$$

where $f(x)$ is the normalized form of $\psi(x)$. The result is that breather frequency, calculated from (3.1) to order a^4, is less than the value (3.8), found from the reduced (3.5) to order a^2. Note that in the case of linear modes (C.1) the a^4 term causes an opposite effect of an increased frequency. After substitution of (C.3) into (C.2) the factor $f_{xx}(0)$ plays the role of an eigenvalue. It is found numerically by applying a shooting method to (C.2) and solving the boundary value problem with the boundary conditions, $\psi(\pm\ \infty)\ =\ \psi_x(0)\ =\ 0$. Instead of a boundary condition at infinity, these constraints are applied at some distant points $\pm x_0$. This is possible due to

the existance of analytic asymptotic solutions at $x \to \pm\infty$ where $\psi(x) \to 0$ and, correspondingly, all β dependent terms in (C.2) can be omitted. This leads to the exponential profile for the breather tail

$$\psi(x) \to C \exp(-\kappa|x|) \qquad\qquad x \to \pm\infty \qquad\qquad (C.4)$$

where the rate of decay, κ, is determined by substitution of exponentially small (C.4) into the equation (C.2) with β-terms ignored, obtaining

$$\kappa^2 = \sqrt{36 \; + \; 72 \; \beta \; {\psi_m}^2 \; - \; f_{xx}(0) \; (1 \; + 9 \; \beta \; \psi_m^2)} \; - \; 6 \qquad\qquad (C.5)$$

Expression (C.5) is valid if $(\; 1 + \; 9 \; \beta \; \psi_m^2) \; {f_{xx}}^2(0) \; < \; 72 \; \beta \; \psi_m^2$ or, equivalently, $\omega^2 > 4$. It is worth mentioning that there exists an exact universal relationship between ω and κ which is valid to all orders of a. Indeed, since $\psi(x) \to 0$ at $x \to \pm\infty$, this asymptotic behavior is described by the linear version of the basic equation (2.4). Substituting the infinite Taylor's series (2.14) into this linear equation and assuming an exponential law of decay (C.4) yields the universal relation

$$\omega \; = \; 2 \; \cosh \frac{\kappa}{2} \qquad\qquad (C.6)$$

This expression is based on the summation of all terms in Taylor's expansion and, correspondingly, it represents an exact result which can also be obtained from the discreet FPU β-model.

The factor $f_{xx}(0)$ is used to estimate the half-width of the bulk envelope function as $\Delta \; \simeq \; |f_{xx}(0)|^{-1/2}$, while κ^{-1} describes the half-width of the tail.

Before numerically solving (C.2) i reproduce analytic results for a breather derived from equation (3.5). The second derivative of (3.17) at $x = 0$ is

$$f_{xx}(0) \;=\; -\,6\;\beta\;\psi_m^2\;/\;(1\;+\;9\;\beta\;\psi_m^2) \qquad (C.7)$$

As is seen from both (C.6) and (3.2) in the a^2 approximation, $\kappa^{-1} = (6\;\beta\;\psi_m^2)^{-1/2}$. The factor Δ, calculated from (C.7), equals κ^{-1} in the small amplitude limit and becomes large, $\Delta = (3/2)^{1/2}$, in the strongly nonlinear regime, indicating that, for large amplitude, the breather envelope function has a two scale structure.

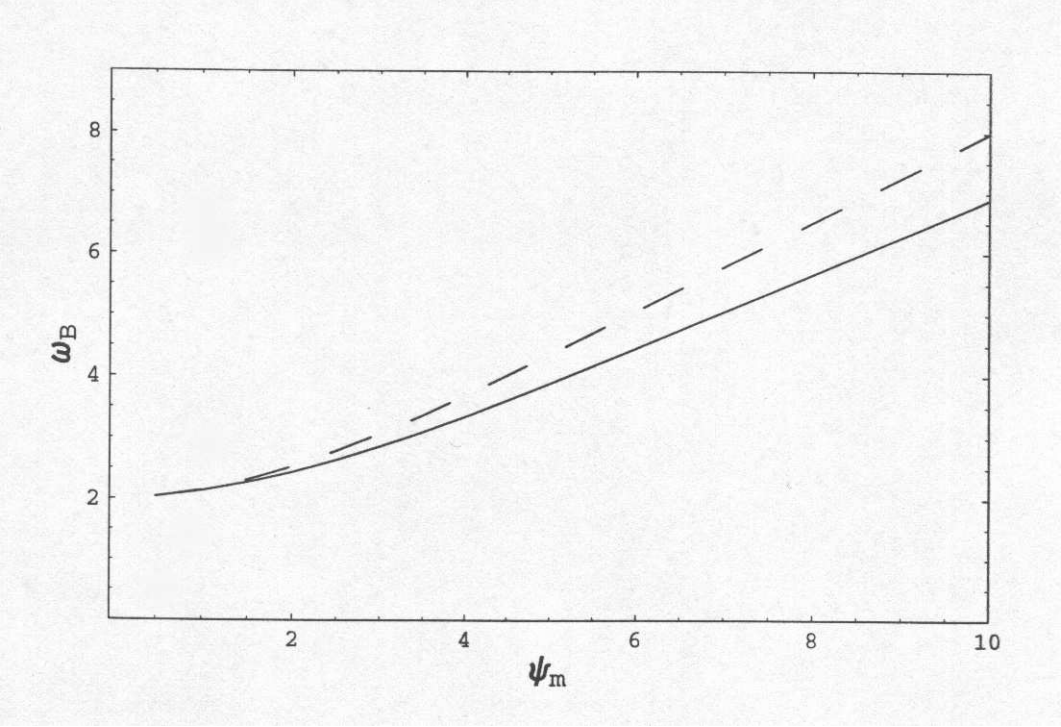

Figure C.1: Dependences of ω_B on breather amplitude, ψ_m; the solid curves correspond to a^4 approximation, the dashed curves to a^2 approximations.

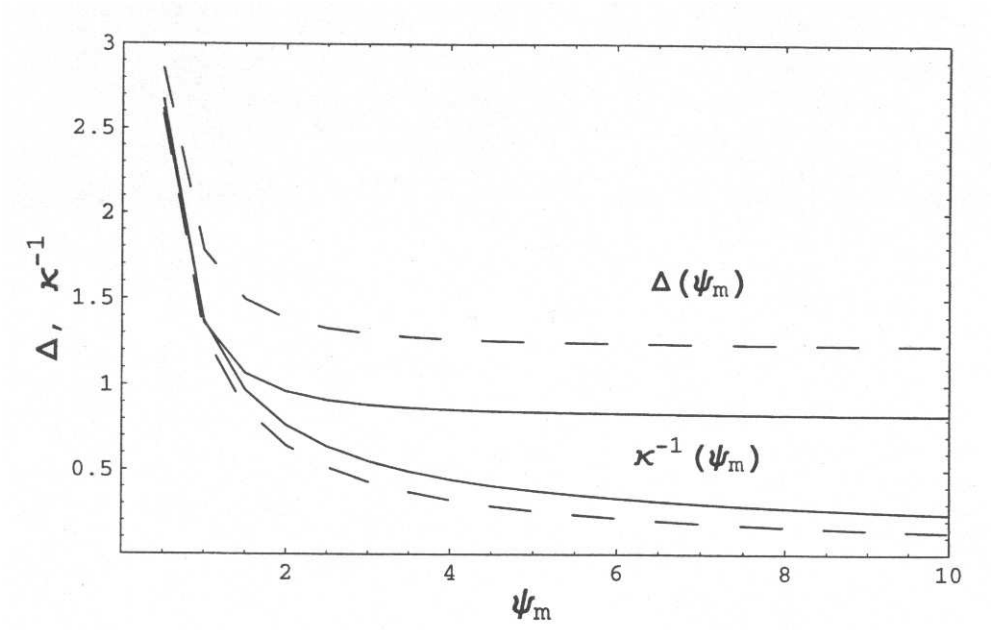

Figure C.2: Dependences of Δ and κ^{-1} on breather amplitude, ψ_m; the solid curves correspond to a^4 approximation, the dashed curves to a^2 approximations.

More detailed quantitative information obtained by numerical integration of (C.2) is presented in Figs. C.1, C.2 which illustrates dependences of ω, Δ and κ^{-1} on ψ_m in both a^2 and a^4 approximations.

The breather profiles described by (3.17) in a^2 approximations and more precise a^4 results based on numerical integration of (C.2) are illustrated in Fig. C.3 for a few typical values of ψ_m. Figs. C.1, C.2 , C.3 show that there is no significant difference between the a^2 and a^4 approximations up to $\psi_m \simeq 2$ which can be considered as the limit of applicability of equation (3.5) and the solution in (3.17). Analytical small amplitude approximation

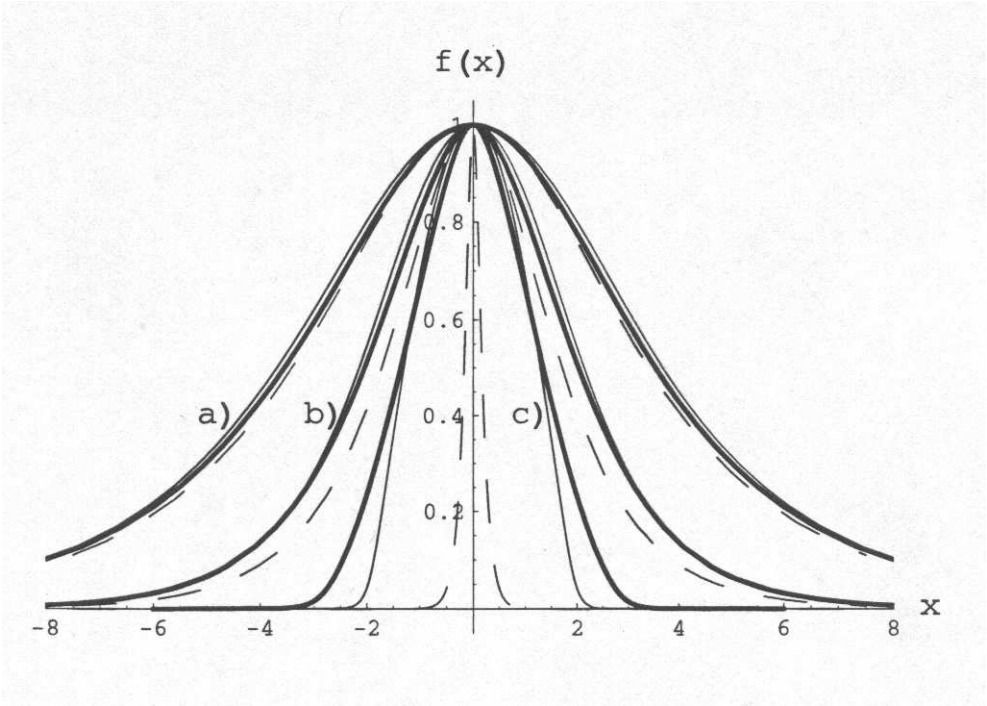

Figure C.3: Comparison of the breather profiles obtained in a^2 approximation (eq. (3.17) - thin solid curves); (eq. (3.18) - dashed curves) and in a^4 approximation (eq. (3.1) - thick solid curves) for three values of the amplitudes; (a) $\psi_m = 0.5$, (b) $\psi_m = 1$, (c) $\psi_m = 10$.

(3.18) is in a good agreement with the numerical curves at lower amplitudes,

$\psi_m \leq 0.5$.

APPENDIX D

ASYMPTOTIC VALUES OF $\mathbf{n_{eff}}$ AND $\mathbf{n_{osc}}$ IN EQUIPARTITION

The effective number of normal modes containing energy is defined by:

$$n_{eff} = \frac{1}{N} \exp\left[- \sum_{j=1}^{j=N} e_j \ln e_j \right] \qquad (D.1)$$

where $e_j = E_j / E_h$ are the normalized linear energies of the normal modes

$$E_j = \Omega_j (Q_j^2 + P_j^2) \qquad (D.2)$$

where $E_h = \sum_1^N E_j$ given by (2.7). Only the quadratic terms in the potential energy are taken into account in (D.2) so that E_h is not total energy E and not exactly conserved during the relaxation. The effective number of oscillators containing energy

$$n_{osc} = \frac{1}{N} \exp\left[- \sum_{i=1}^{i=N} e_i \ln e_i \right] \qquad (D.3)$$

is based on the normalized oscillator energies $e_i = E_i / E$ which includes all terms so that $\sum_1^N E_i$ is conserved exactly

$$E_i = \frac{1}{2} {p_i}^2 + \frac{1}{4}[(q_{i+1} - q_i)^2 + (q_i - q_{i-1})^2] + \frac{\beta}{8}[(q_{i+1} - q_i)^4 + (q_i - q_{i-1})^4] \qquad (D.4)$$

Depending on the relative variations of energies $e_{i,j}$, from one mode or oscillator to another, the values of n_{eff} or n_{osc} vary in the range from $1/N$ to 1. The upper limit corresponds to equipartition state where all e_i and e_j are the same and equal to $1/N$. Numerical curves plotted in Fig. 6.3, 6.4, for $N = 128$ and $E = 50$ give asymptotic values at $t \to \infty$ of $n_{eff} = 0.61$ and $n_{osc} = 0.715$, which are lower than the upper limit values $n_{osc} = n_{eff} = 1$, as expected due to the fluctuations of energies $e_{i,j}$ caused by interaction between modes (oscillators). In order to calculate the effect i introduce a deviation $\delta e_{i,j}$ from equipartition

$$e_{i,j} = \overline{e_{i,j}} + \delta e_{i,j} \qquad (D.5)$$

Subsituting (D.5) into (D.1) or (D.2), expanding the logarithmic function, which holds both for modes and oscillators, as $\ln(1 + \delta e_i/\overline{e_i}) = \delta e_i/\overline{e_i} - (1/2)(\delta e_i/\overline{e_i})^2$ and performing the summation over i yields

$$n_{eff} = n_{osc} = \frac{1}{N} \exp\ \{-N\overline{e} \ln \overline{e} - N\overline{\delta e^2}/(2\overline{e})\} = \exp\ \{-N\overline{\delta e^2}/(2\overline{e}\} \qquad (D.6)$$

Taking $\overline{e} = 1/N$ and making the assumption of normal statistics that for each normal mode $\overline{\delta e^2} = \overline{e}^2$ (this is confirmed by calculations), gives an asymptotic value $n_{osc} = n_{eff} = \exp(-0.5) = 0.61$. This calculation illustrates why the result does not depend on the number of oscillators if N is sufficiently large and is in apparent good agreement with the numerical

simulation for n_{eff}, but not for n_{osc}.

For an alternative perspective, from statistical mechanics we note that the sums on the R.H.S. of (D.1), (D.2) can be treated as ensemble averages of the function $e \ln e$ (if, of course, modes (oscillators) are statistically independent)

$$\overline{e \ \ln e} \ = \frac{1}{N} \sum_{i=1}^{i=N} e_i \ln e_i \qquad (D.7)$$

The L.H.S of (D.7) is calculated as a mean value of $e \ln e$ averaged over accesible states of the normal mode (oscillator) which are smoothly distributed in the phase space due to energy exchange with the rest of the $N-1$ modes. They play the role of a heat reservoir while the total energy of the combined system is conserved. In this situation a canonical distribution can be used to describe probabilities of the different states of a single normal mode (oscillator).

For the normal modes the canonical distribution has a form

$$d\mathcal{P} = \frac{1}{Z} \exp\{-\frac{E_j(P,Q)}{T}\} \ dP \ dQ \qquad (D.8)$$

where $d\mathcal{P}$ is the probability of finding the mode in the state P, Q, and the partition function Z is defined by the normalization condition

$$Z = \int_{-\infty}^{\infty} \int_{-\infty}^{\infty} \exp \ \{-\frac{E_j(P,Q)}{T}\} \ dP \ dQ \qquad (D.9)$$

The effective temperature of the heat bath T is chosen such that $\overline{E_j} = E/N$ with E_j given by (D.2). Performing the integration over P and Q yields an

expression for Z. The mean value of E_j is then calculated as

$$\overline{E_j} = \frac{1}{Z}\int_{-\infty}^{\infty}\int_{-\infty}^{\infty} E_J(P,Q)\exp\ \{-\frac{E_j(P,Q)}{T}\}dP\ dQ \equiv T \qquad (D.10)$$

where $T = E/N$ is the effective temperature. Substituting these results into the integral for the mean value of $e\ln e$ yields

$$\overline{e\ln\ e} = \frac{1}{N}\int_0^{\infty} x\ \ln(x/N)\exp(-x)\ dx \qquad (D.11)$$

Multiplying (D.11) by N and subsituting in (D.1) gives an expression for the asymptotic value of n_{eff}

$$n_{eff}(\infty) = \frac{1}{N}\exp[-N\ \overline{e\ln e}] = 0.6552 \qquad (D.12)$$

which does not depend on N. This limit is rather close to numerical value 0.61 but slightly exceeds it. The relative difference of the order of 0.08 cannot be explained by the fact that only the quadratic part of potential energy is taken into account. If $E = 50, N = 128$ then the relative value of the quartic term with respect to the total energy of the mode is $\beta\ E/(4\ N) \simeq 0.01$ which is too small to explain the difference observed.

In the case of oscillators the canonical distribution has a more complicated form because the energy of each oscillator i depends formally on four variables $p_i,\ q_{i-1},\ q_i,\ q_{i+1}$ (see, Eq.(D.4)). Correspondingly, the partition function and all mean values are defined by mulidimensional integrals. Since the potential energy is a function of differences $q_{i+1} - q_i,\ q_i - q_{i-1}$,

the number of independent variables for integration is reduced to 3: $x = q_{i+1} - q_i$, $y = q_i - q_{i-1}$ and $p = p_i$. Correspondingly, expressions for Z, the mean values of E_i, and $e \ln e$ take the form

$$Z = \int_{-\infty}^{\infty} \int_{-\infty}^{\infty} \int_{-\infty}^{\infty} \exp \{-\frac{E_i(p,x,y)}{T}\} \, dp \, dx \, dy \qquad (D.13)$$

$$\overline{E_i} = \frac{1}{Z} \int_{-\infty}^{\infty} \int_{-\infty}^{\infty} \int_{-\infty}^{\infty} E_i(p,x,y) \exp \{-\frac{E_i(p,x,y)}{T}\} \, dp \, dx \, dy \qquad (D.14)$$

$$\overline{e \ln e} = \frac{1}{Z} \int_{-\infty}^{\infty} \int_{-\infty}^{\infty} \int_{-\infty}^{\infty} \left(\frac{E_i(p,x,y)}{E}\right) \ln \left(\frac{E_i(p,x,y)}{E}\right) \exp \{-\frac{E_i(p,x,y)}{T}\} dp \, dx \, dy \qquad (D.15)$$

where

$$E_i(p,x,y) = \frac{1}{2} {p_i}^2 + \frac{1}{4}(x^2 + y^2) + \frac{\beta}{8}(x^4 + y^4) \qquad (D.16)$$

The equations are integrated numerically. Given an effective temperature T, the number of oscillators N and total energy E, the mean value of energy per oscillator $\overline{E_i}$ is found from (D.14). Equating $\overline{E_i}$ to its equipartition value, E/N, yields an appropriate effective temperature which is then used to calculate $\overline{e \ln e}$. This leads to the asymptotic value of $n_{osc}(\infty) = 0.74$ that slightly exceeds the result of numerical calculations.